



MASTER THESIS PROJECT

Relating horizontal subsurface microplastic movement to surface fields in the North Atlantic

Judith Marina Ewald

Institute for Marine and Atmospheric Research (IMAU) at Utrecht University

Supervisors: Dr. Erik van Sebille and Dr. Philippe Delandmeter

PLENTZIA (UPV/EHU), SEPTEMBER 2019



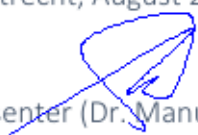
Dr. Manu Soto as teaching staff of the MER Master of the University of Basque Country

CERTIFIES:

That the research work entitled

'Relating horizontal subsurface microplastic movement to surface fields in the North Atlantic'
has been carried out by Judith Marina Ewald
at the Institute for Marine and Atmospheric research Utrecht (IMAU, University of Utrecht)
under the supervision of Dr. Erik van Sebille
in order to achieve 30 ECTS as a part of the MER Master program.

In Utrecht, August 2019


Presenter (Dr. Manu Soto)




Supervisor (Dr. Erik van Sebille)

PLENTZIA (UPV/EHU), SEPTEMBER 2019

Acknowledgements

First of all, I like to acknowledge my supervisors Dr. Erik van Sebille and Dr. Philippe Delandmeter for their continuous guidance during the project. They helped me to find back to the red line when I started drifting like a piece of plastic in the ocean. Furthermore, I would like to thank the whole TOPIOS research team and fellow IMAU students for a warm welcome to Utrecht, their helpful suggestions and the inspiring insights into their work. Here goes one special thank you to Anneke, who helped me during my first weeks of orientation and more. Then, I would like to thank Dr. Jon Saenz for helping me to find a project. Moreover, I would like to thank the fellow MER students for their friendship and fruitful exchanges. One special thank you to Darshika as her explanations about coding lead to more than one enlightenment. Finally, I would like to thank my family and friends for their support, and especially Tim, who has been an island in the ocean.

Contents

1	Summary	1
2	Second Language Summary	2
3	Introduction	4
3.1	Ocean PARCELS - Lagrangian Ocean Analysis	6
3.2	SKIM Satellite	6
3.3	Scope of the project	8
4	Methods	9
4.1	Simulations	9
4.2	Post-Processing	12
5	Results	16
5.1	Simulations	16
5.2	Post-Processing	17
5.2.1	Correlations	20
6	Discussion	28
7	Conclusion	32
8	Annexes	37
8.1	Figures	37
8.2	Scripts	46



Utrecht University

1 Summary

Marine microplastics (MP) are a major concern investigated in all disciplines of marine sciences, since they are a threat to marine life, carry toxic substances and can transport invasive species through the oceans (Andrady 2011, Lei et al. 2017). Even with joint efforts from many scientists, policy makers, and citizen scientists from all over the world, there are still knowledge gaps regarding the fate of plastic entering the ocean such as the pathways and accumulation (Van Sebille et al. 2015, Hardesty et al. 2017).

Hence, there is a need of instruments with the capability to increase the quality of MP quantification. The proposed ESA (European Space Agency) satellite mission SKIM will be able to measure the Stokes drift, which is needed to increase the accuracy of total surface current measurements (Ardhuin et al. 2019, Onink et al. 2019). This development can help to increase the accuracy of Lagrangian surface simulations, since flow fields from Eulerian measurements and models are used for the advection of virtual particles (Onink et al. 2019). Virtual particles can represent many kinds of marine debris such as MP.

However, this only accounts for surface simulations. This thesis investigates if two-dimensional surface measurements can be used to derive three-dimensional sub-surface flows of MP in the North Atlantic. Therefore, the Lagrangian Ocean Analysis PARCELS (Probably A Really Computationally Efficient Lagrangian Simulator) (Lange and Van Sebille 2017) is used to simulate particles advected by meridional and zonal NEMO (Nucleus for European Modelling of the Ocean) flow-fields.

One surface simulation and two sub-surface simulations are performed. The sub-surface MP-particle flows are simulated by applying the empirical models for vertical mixing developed by Kukulka et al. (2012) and Poulain et al. (2019). The simulation based on the model from Poulain et al. (2019) is characterised by a rise velocity of one magnitude lower than the rise velocity of the simulation based on the model from Kukulka et al. (2012). Then, the travelled particle distances and directions after 3 days are calculated, since SKIM is designed to have an orbit time of 8 hours to 4 days days. Moreover, the differences between these distances and directions of surface and sub-surface trajectories are computed.

The differences in changes of direction show a less significant result than the differences between distances. Even though the differences in distances show a certain pattern, the differences in changes of direction are not spatially co-appearing with certain patterns of the North Atlantic. Specifically, the differences between distances increase along the strong ocean currents of the North Atlantic such as the Gulf Stream. And in four of five investigated subsections of the North Atlantic, the differences in distances increase with increasing particle depths of the sub-surface simulations.

Overall, the surface and sub-surface MP-flows differ, but essentially in distinctive regions. And the correlations of the differences in distances and a range of NEMO variables, e.g. mixed layer depth (MLD), do not indicate a strong relationship, but the two-dimensional histograms allow some hypothesis on the relationships. The differences in distances of horizontal sub-surface and surface trajectories are not directly correlated to increasing depth due to downward mixing, but to the changes in ocean dynamics with increasing depth. And as the dynamics and their variability vary spatially, the differences vary spatially.

2 Second Language Summary

Mariene microplastics (MP) worden in de disciplines van de mariene wetenschappen onderzocht, omdat ze een bedreiging vormen voor het mariene leven, giftige stoffen dragen en invasieve soorten kunnen transporteren (Andrady 2011, Lei et al. 2017). Zelfs met gezamenlijke inspanningen van wetenschappers, beleidsmakers en amateurwetenschappers van over de hele wereld, zijn er nog steeds kennislacunes over het verblijf van MP, zoals de baanen en de accumulatie (Van Sebille et al. 2015, Hardesty et al. 2017).

Daarom is er behoefte aan instrumenten die de kwaliteit van MP-kwantificering kunnen verbeteren. De voorgestelde ESA (European Space Agency) satellietmissie SKIM zal de Stokesdrift kunnen meten, wat nodig is om de nauwkeurigheid van de stromingsmetingen van het oceaanoppervlak te vergroten (Ardhuin et al. 2019, Onink et al. 2019). Deze ontwikkeling kan helpen de nauwkeurigheid van Lagrangiaanse oppervlaktesimulaties te vergroten, omdat stromingvelden van Euleriaanse metingen en modellen, zoals satellietmetingen, voor de advectie van virtuele deeltjes in Lagrangiaanse simulaties gebruikt worden (Onink et al. 2019). Virtuele deeltjes kunnen vele soorten zeeafval vertegenwoordigen, bijvoorbeeld MP.

Dit houdt alleen rekening met oppervlaktesimulaties. Deze proefschrift onderzoekt of tweedimensionale oppervlaktemetingen kunnen gebruikt worden om driedimensionale MP-stromen in het Noord-Atlantische gebied af te leiden. Daarom wordt de Lagrangiaanse oceaansimulator PARCELS (Probably A Really Computationally Efficient Lagrangian Simulator) (Lange and Van Sebille 2017) gebruikt om deeltjes met de meridionale en zonale NEMO (Nucleus for European Modelling of the Ocean) stromingsvelden te simuleren.

Er zijn een oppervlaktesimulatie en twee suboppervlaktesimulaties uitgevoerd. De MP-deeltjes die onder het oppervlak bewegen worden door toepassing van empirische modellen voor verticaal mengen, ontwikkeld door Kukulka et al. (2012) en Poulain et al. (2019), gesimuleerd. De simulatie op basis van het model van Poulain et al. (2019) wordt gekenmerkt door een MP-stijgsnelheid van een grootte lager dan de stijgsnelheid van de simulatie op basis van het model van Kukulka et al. (2012). Vervolgens worden de afgelegde afstanden en richtingen van de deeltjes na 3 dagen berekend, omdat SKIM ontworpen is om een omlooptijd van 8 uur tot 4 dagen te hebben. Verder worden de verschillen tussen deze afstanden en richtingen van oppervlakte- en suboppervlakte banen berekend.

De verschillen in richtingsveranderingen vormen een minder significant resultaat dan de verschillen tussen de afstanden, en de verschillen in richtingsveranderingen overlappen niet met bepaalde patronen van de Noord-Atlantische Oceaan. De verschillen tussen afstanden zijn significant langs de sterke zeestromingen van de Noord-Atlantische Oceaan, zoals de Golfstroom. Daarnaast neemen in vier van de vijf onderzochte subsecties van de Noord-Atlantische Oceaan de verschillen in afstanden met toenemende deeltjesdiepten toe.

De oppervlakte- en suboppervlak MP-stromen wijken van elkaar af, maar variëren met de ruimtelijke condities. En de correlaties van de verschillen tussen de afstanden en de NEMO-variabelen, b.v. diepte van gemengde laag (MLD), duiden niet op een sterke relatie, maar de tweedimensionale histogrammen

laten ruimte voor hypothese over de relaties toe. De verschillen in afstanden tussen trajecten in het horizontale suboppervlak en trajecten aan het oppervlakervlak zijn niet direct gecorreleerd met toenemende diepte, als gevolg van neerwaartsemenging, maar wel met de veranderingen in oceaandynamica met toenemende diepte. Aangezien die dynamiek en diens variabiliteit ruimtelijk variëren, varieren de verschillen tussen het oppervlak en suboppervlak ook ruimtelijk.

3 Introduction

Numerous scientists and projects are dedicated to estimating the amount and distribution of plastic debris in the ocean. Since plastic debris of all sizes and shapes is a threat to marine life, this global issue gathers an increasing, global attention from scientists, policy makers, and the general public (Andrady 2011). The estimation of a global annual input of plastic into the ocean is 4.8 - 12.7 million metric tons (MT) in 2010 (Jambeck et al. 2015). Van Sebille et al. (2015) estimated, based on a range of studies, a mass of 93 - 236 MT of accumulated microplastic in the global ocean in 2014. However, this only accounts for about 1% of the global annual input of 2010 estimated by Jambeck et al. (2015). This discrepancy reflects the knowledge gaps in sources, pathways, distribution and accumulation of MP in the marine environment.

Due to currents, Ekman-transport and Stokes-drift, marine debris tends to gather in the so called garbage patches, which are located within vast gyres (Law et al. 2010, Lebreton et al. 2018). The Stokes drift was first described about 170 years ago and is defined as the net drift velocity of a floating particle at a free water surface in the direction of wave propagation during the periodic motion (Craik 2005). It can also be described as the difference of the average Lagrangian flow velocity of a fluid parcel and the average Eulerian flow velocity of that fluid (Van den Bremer and Breivik 2018). As buoyant plastic particles float at the ocean surface and within the upper ocean layer, they experience continuous disposition due to the Stokes drift (Van den Bremer and Breivik 2018).

MP is defined as plastic with a diameter < 5 mm, and can be grouped into primary and secondary MP. Primary MP is mainly an industrial basic material, whereas secondary MP forms due to degradation of larger pieces (Cai et al. 2018). Weathering of plastic and its degradation into MP is forced by UV-radiation, physical stress, wave action, salinity, fluctuating temperatures, biofilm formation and microbial degradation (Jahnke et al. 2017) .

Due to a relatively low density of MP debris (e.g. 965 kg/m³, Kukulka et al. 2012) in comparison to seawater (\sim 1026 kg/m³), particles experience buoyancy, but also downward mixing driven by wind, waves and other processes such as convergence and Langmuir circulation (Kukulka et al. 2012, Reisser et al. 2015). Rise velocity due to buoyancy depends on the type and size of the given particle. Reisser et al. (2015) and Kukulka et al. (2012) both observed that plastic particle density concentrations decrease exponentially with depth and that depth decay rates decrease with increasing wind speed determining the sea state. Poulain et al. (2019) investigated how to estimate the concentration in count and mass of particles in the water column by extrapolating surface samples. Their laboratory measurements show that smaller particles have a significantly smaller rise velocity than larger MP. Enders et al. (2015) found that small microplastics (SMP; <1 mm) can be transported downwards to hundred meters depths, while large microplastics (LMP; 1 mm to 5 mm) can be mixed down only over a few meters at the same sea state. Poulain et al. (2019) distinguishes SMP (25 μ m to 1000 μ m) from LMP (1 mm to 5 mm) as well, and

additionally takes the particle shape as a factor, influencing the rising velocity of MP, into account. Likewise Kukulka et al. (2012), Poulain et al. (2019) developed an empirical model for the vertical motion of MP due to downward forcing turbulence and rise velocity due to buoyancy. They concluded that sampling the surface layer alone to estimate the amount and mass of microplastics is insufficient. Thus, empirical models can be used to extrapolate surface samples over depth.

However, the ocean dynamics change with depth, due to Ekman transport for instance. The Ekman theory was developed in 1905 by the Swedish scientist W. V. Ekman and he assumed a steady wind stress over an ocean which is infinitive in depths and widths. Hence, friction occurring at boundaries like the bottom and horizontal boundaries, such as the ocean-continent boundaries, are ignored. Moreover, pressure gradients and density inhomogeneity are not taken into account. The Ekman-spiral model is based on a balance among the Coriolis-force, viscous friction and the pressure gradient. This leads to a current at the ocean surface which travels 45° to the right in the Northern hemisphere and to the left in the Southern hemisphere. The direction and speed of the water changes with depth, thus each layer underneath another layer turns a bit more to the right (left in the Southern hemisphere) and decreases in speed due to the Coriolis effect and friction, respectively. The average direction and speed over depth is called the Ekman-transport. Even though the Ekman spiral was measured in laboratory experiments of laminar flows, it is rarely observed in the marine environment. Due to the relatively low speed of the Ekman-transport in comparison to geostrophic currents, and the high-frequency wave-induced surface transport which adds noise to the measurements, measuring the Ekman-transport in the ocean remained impossible for decades. However, Weller and Plueddemann (1996) and Schudlich and Price (1998) measured current and wind speed simultaneously and found that the near-surface water volume transport is consistent with the Ekman-transport.

As the flow conditions change with depth, it generates a more sufficient and representative result to use a three-dimensional flow-field carrying MP and taking vertical mixing as well as rotational forces into account, than surface transport only. The Ocean General Circulation Model (OGCM) NEMO (Nucleus for European Modelling of the Ocean) is a primitive equation ocean model with a three-dimensional velocity field and the capability of modelling the Ekman-transport (Madec 2008). The horizontal fields are provided on a curvilinear orthogonal grid and the vertical direction is provided as a z- or s-coordinate (Madec 2008).

This thesis investigates how two-dimensional surface flows can be used to estimate three-dimensional horizontal sub-surface flows in the North Atlantic. In this case, two-dimensional flows are MP-trajectories advected by zonal and meridional velocities. Three-dimensional flows are MP-trajectories advected by zonal and meridional velocities, which may experience a change of direction with depths, plus vertical mixing forced by wind and buoyancy.

3.1 Ocean PARCELS - Lagrangian Ocean Analysis

Lagrangian Ocean analysis simulates particle pathways, and the particles can represent various floating and non-floating particle types of ocean-origin, like larvae, kelp and microplankton, but also particles of anthropogenic sources, such as plastic (Singh et al. 2018, Nooteboom et al. 2019, Hardesty et al. 2017).

Parcels (Probably A Really Computationally Efficient Lagrangian Simulator) is a set of Python methods and classes to track particles through hydrodynamic fields from OGCMs such as NEMO (Lange and Van Sebille 2017). Solving the following equation:

$$X(t + \Delta t) = X(t) + \int_t^{t+\Delta t} v(x, \tau) d\tau + \Delta X_b(t), \quad (1)$$

describes the computation of Lagrangian particle trajectories. X is the three-dimensional particle position, $v(x, \tau)$ is the three-dimensional velocity field at position X from a hydrodynamic field imported from a OGCM. And $\Delta X_b(t)$ is the particle behaviour, for instance buoyancy (Lange and Van Sebille 2017).

The general structure of Parcels is subdivided into a range of classes and methods. The *Fields* objects hold the hydrodynamic data, which is structured with longitude, latitude, depth and time. The *FieldSet* object contains the *Fields* objects and holds a minimum requirement of U (zonal velocity) and V (meridional velocity) to work. Likewise the *FieldSet* object, *Particle* objects contain information like longitude, latitude, depth and time to characterise the virtual particles. Finally, a *ParticleSet* object merges the information of the *FieldSet* and the *ParticleSet*. With the *ParticleSet.execute* method, the simulation starts (Lange and Van Sebille 2017). Parcels provides the option of implementing custom kernels. With these kernels the behaviour of the particles can be defined. Hence, particles can be of passive or active type. Moreover, PARCELS implies an interpolation scheme for a three-dimensional curvilinear C-Grid, which is required to use the curvilinear NEMO-fields. (Delandmeter and Van Sebille 2019)

3.2 SKIM Satellite

Satellite altimeters are capable to measure dynamic variables as along-track sea level anomalies and significant wave heights, but there is a lack of measuring kinematic variables which are acting at a smaller scale than dynamic variables. SKIM (Sea Surface KInematics Multiscale Monitoring, <https://www.skim-ee9.org/>), a satellite proposed to be the European Space Agency's "Earth Explorer 9", uses Doppler technique (upshifted vs. downshifted signals) combined with a nadir (0°) and off-nadir (6° , 12°) incidence angle beams. The incidence angle beams allow measuring a directional wave spectrum down to wavelengths of 30 m. Wave spectra can be used to estimate the wave induced Stokes drift to correct for the Doppler velocity. Thus, the

surface velocity vector corrected for the Stokes drift can be observed. The expected accuracy on horizontal current velocity is 0.07 m/s for horizontal wavelengths larger than 80 km. The revisit time of SKIM will be 8 hours to 4 days (Ardhuin et al. 2018, Ardhuin et al. 2019). As SKIM is still under development, the technical properties as well as the temporal and spatial resolution of the data output might be further adjusted. Note that the horizontal velocity accuracy is expected to be lower in the gyres as the currents are weaker in these areas. Moreover, the expected distance to the coastline from which measurements are possible is about 30 km.

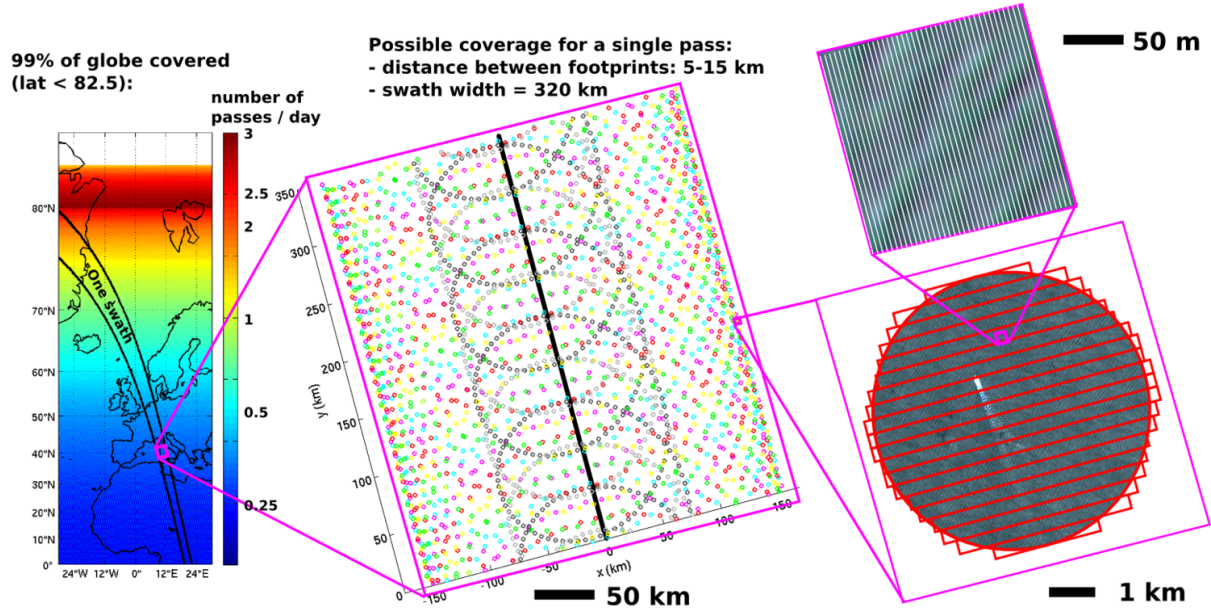


Figure 1: Spatial scales of SKIM measurements. From the smallest to the largest scale: The smallest scale represents the wind-generated wave data measured with Doppler technology. The circle represents a footprint with a diameter of 6 km. These footprints can be separated into azimuthal strips with a 300m-resolution which is indicated with the red boxes. One scale larger one can see the 320 km wide swath. The dots are the footprints which are sparsely distributed along the swath with a distance of 5 - 15 km to each other. Here, the black line shows the nadir radar beam, the coloured dots show the 12° incidence angle radar beams and the grey dots represent the 6° incidence angle radar beams as explained in the text. The image with the largest scale shows that the revisit time varies with latitudes. With a 824 km altitude orbit the revisit time is between 8 hours and 4 days. Source: Ardhuin et al. (2019)

As Lagrangian ocean analysis is very sensitive to the accuracy of flow fields (Onink et al. 2019), the combination of the surface currents measurements and the Stokes drift, as proposed by the SKIM mission, would increase the accuracy of analysing and simulating the pathways of marine debris such as MP (Ardhuin et al. 2019).

3.3 Scope of the project

Since SKIM is not launched yet, there is no measured data available. However, an analysis of the transport of MP by surface currents versus the transport of MP by sub-surface currents including vertical mixing and buoyancy, can give insight of the potential to use two-dimensional SKIM measurements to model three-dimensional MP transport. Thus, Parcels is used to simulate two-dimensional NEMO surface flows and particle trajectories, but also three-dimensional NEMO flow fields and corresponding particle trajectories (Delandmeter and Van Sebille 2019). NEMO is used to model the Ekman transport and I implied particle behaviour as buoyancy and downward mixing due to wind stress τ . Therefore, I used the empirical models developed by Kukulka et al. (2012) and Poulain et al. (2019) to define the particle behaviour within a Parcels custom kernel. Then, in order to investigate the differences of the surface and sub-surface flows, the polar coordinates of the surface and horizontal sub-surface flows are calculated using the Haversine formula for the distance. A point wise correlation of various NEMO variables as such as wind stress τ and mixed layer depth (MLD) is performed. Finally, the interpretation of the results seeks to find the potential of gathering sub-surface flows from surface flows, and to find physical processes which are leading to differences of surface and sub-surface flows. The North Atlantic determined is target area, because there is a great potential of integrating the Stokes-flow into modelling approaches of this area (Onink et al. 2019).

The research questions of this thesis are: (1) Is there a difference of surface and sub-surface MP-flows in the North Atlantic? (2) If yes, what are the driving forces leading to the difference? (3) And finally, can a 2D-product such as SKIM surface measurements be used to track 3D-flows?

4 Methods

4.1 Simulations

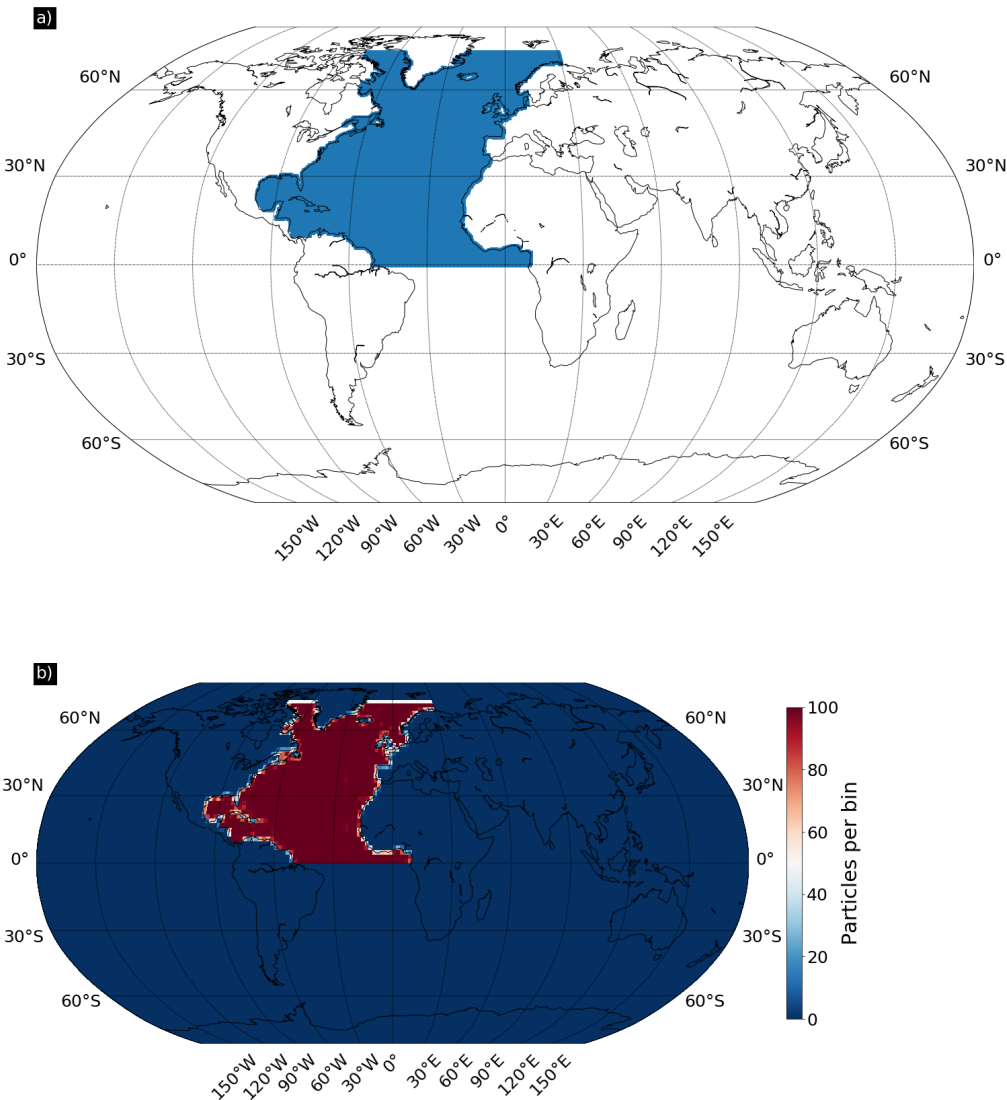


Figure 2: Initial grid of the particles. a) Shows distribution of 122622 particles in North Atlantic; b) presents particles per bin: The distribution should be consistent everywhere but on land.

The simulations of microplastic trajectories are modelled with the Lagrangian Python method OceanParcels version 2.0.0-beta (Lange and Van Sebille 2017, oceanparcels.org). In this case, the Python version 3.6 is used. The standard run NEMO-N006 of the Ocean Circulation model NEMO (Madec 2008) provides the zonal and meridional velocities (U , V), and wind stress τ fields on an ORCA grid. The fields are used to construct the FieldSet objects with OceanParcels. The resolution of the fields is $1/12^\circ$ and a 5-day mean (Madec and Imbard 1996). The time interpolation is carried out with linear interpolation, and space interpolation of the fields to the particle positions is performed with a C-grid interpolation scheme (Delandmeter and Van Sebille 2019). The 4th order Runge–Kutta method (RK4), is already implemented in Parcels and applied for the 2D as well as for 3D simulations. For the 3D simulation with vertical mixing all 75 depth level of the NEMO model are used for the FieldSet object. Initially, the particles are regularly distributed at the surface as a $0.2^\circ \times 0.2^\circ$ grid. The initial grid covers the whole simulation field of the North Atlantic from 0° North to 75° North and from 100° West to 30° East (Figure 2).

Reisser et al. (2015) and Kukulka et al. (2012) both observed that plastic particle density concentrations decrease exponentially with depth and that depth decay rates decrease with increasing wind speed determining the sea state. Kukulka et al. (2012) investigated the vertical fluxes of microplastics in the oceanic water column due to wind stress τ . They developed an empirical model containing a turbulent eddy exchange coefficient (A_0) and buoyancy (ω). It can be written as

$$n(z) \propto \exp(-\lambda z) \quad (2)$$

where the depth decay rate $\lambda = \omega/A_0$ and $A_0 = 1.5u_{*\omega}\kappa H_s$ with $u_{*\omega}$ as frictional water velocity, $\kappa = 0.4$ as Karman constant, $H_s = 0.96g^{-1}\sigma^{(3/2)}u_{*a}^2$ with g as gravitational constant, σ as wave age, u_{*a}^2 as frictional air velocity, and as in Kukulka et al. (2012) $\sigma = 35$. The frictional air velocity is assigned as $u_{*a}^2 = \sqrt{|\vec{\tau}|/\rho_a}$ with wind stress τ and air density $\rho_a = 1.22 \text{ kg/m}^3$. For the frictional water velocity $u_{*w}^2 = \sqrt{|\vec{\tau}|/\rho_w}$ with $\rho_w = 1027 \text{ kg/m}^3$. Thus, $A_0 = 0.31 \cdot |\vec{\tau}|^{3/2} \text{ m}^2\text{s}^{-1}$. The magnitude of wind stress $|\tau|$ is given in Pa provided by the NEMO dataset. Therefore, a custom kernel is implemented in Parcels.

Kukulka et al. (2012) defined buoyancy (ω) as a range of $0.005 - 0.035 \text{ m/s}$, depending on particle shape, size and density, water turbulence and drag forces. In the simulation named 'Kukulka' the rise velocity is defined as $\omega = 0.005 \text{ m/s}$, which is a relatively low rising velocity value measured by Reisser et al. (2015). Reisser et al. (2015) studied the vertical distribution of buoyant plastics in the North Atlantic Gyre. They found that plastic concentration drop exponentially with water depths, and that decay rates decrease with increasing Beaufort scale, hence wind speed. Moreover, smaller pieces were more susceptible to vertical transport. Due to this findings they performed experimental measurements of the rise velocity with a focus on the evaluation of type and size of the plastic pieces. They concluded that the vertical mixing

process is size selective and results in a size-distribution of smaller particles with greater depths, because smaller particles have a smaller rise velocity. The relation of the rise velocity and the size and type of the plastic pieces was analysed for macroscopic plastic pieces of a size range from 0.5 mm to 207 mm (Reisser et al. 2015). Kukulka et al. (2012) uses data from surface Neuston net tows with a 335 µm mesh. Thus, Kukulka et al. (2012) takes smaller pieces into account than Reisser et al. (2015). The major difference between the results of Kukulka et al. (2012) and Reisser et al. (2015) is the particle distribution at the calmest sea state (Beaufort scale 1): Kukulka et al. (2012) found that all particles were concentrated at the surface, whereas Reisser et al. (2015) measured particles submerged to a depth of about 0.5 m. However, this could also be due to rising plastic from deeper layers or other vertical flows.

Applying the results of measurements carried out by Poulain et al. (2019), we take a lower buoyancy $\omega = 0.00049 \text{ m/s}$ for the simulation 'Poulain'. Please note that this rising velocity is of one magnitude lower in the simulation 'Kukulka'. This is due to the different approaches of the studies: With a minimum of 25 µm Poulain et al. (2019) take much smaller pieces into account than the other studies explained above. The rise velocity is calculated with the model developed by Poulain et al. (2019)

$$\frac{1}{2}\rho C_D(Re)SW_b^2 = (\rho_p - \rho)Vg \quad (3)$$

where ρ = fluid density, ρ_p = particle density and C_D = Drag coefficient. Re is the Reynolds number and calculated with $\frac{L \cdot W_b}{\nu}$, where L is a characteristic length scale, W_b a characteristic velocity and ν = kinematic viscosity. The definition of L and W_b are explained in detail in Poulain et al. (2019). S is the area of the apparent section of the particle. Finally, V is the particle volume and g is the gravitational constant. Poulain et al. (2019) distinguish small microplastics (SMP) from large microplastics (LMP), with particle volume ranges V of 0.0025 mm to 1 mm, and 1 mm to 5 mm, respectively. Moreover, they differentiate between shapes through assigning $\rho_p = 0.9 \text{ g/cm}^3$ to a spherical shape and $\rho_p = 1.005 \text{ g/cm}^3$ to an ellipsoidal shape. Considering an ellipsoidal shape and the smallest value for $V = 0.0025 \text{ mm}$ (SMP) leads to $\omega = 0.00049 \text{ m/s}$. Even though Poulain et al. (2019) found that about 95% show a geometry defined as a sphere, I consider an ellipsoidal shape due to the lower rise velocity. The aim is here to consider extreme values in order account for the whole range of possible MP characteristics, and to examine the difference of the models proposed by Kukulka et al. (2012) and Poulain et al. (2019). And since Poulain et al. (2019) found that for a given density ellipsoidal particles rise slower than spherical particles, they attributed ellipsoidal shapes to a higher density than spherical shapes.

Table 1: Simulations in Ocean Parcels

Simulation	Parameters
Surface	No vertical mixing
Kukulka	$p(z) = \lambda e^{-\lambda z}$ and $\omega = 0.005$ m/s
Poulain	$p(z) = \lambda e^{-\lambda z}$ and $\omega = 0.00049$ m/s

As Parcels works with spherical meshes, a converter needs to be applied in order to track particle velocities in m/s instead of degrees/sec. Hence, a unit converter kernel is used. The conversion for the U velocity field is

$$1852 \cdot 60 \cdot \cos(lat \cdot \frac{\pi}{180}), \quad (4)$$

and the conversion of the V velocity field is

$$1852 \cdot 60. \quad (5)$$

Since the orbit time of SKIM is 3 days, the simulation time is defined as 3 days with an output each 3 hours. The NEMO data is a 5 day mean from the 10th of January 2010. So the NEMO flow field does not vary in time and the date is chosen randomly.

4.2 Post-Processing

For plotting the output the Python package Matplotlib (Hunter 2007) is used. In order to compare and analyse the particle trajectories of the surface and sub-surface simulations, the polar coordinates of each particle for all time-steps are calculated. For better understanding, this method is performed on a set of 270 particles (Figure 3) before applying it to the whole set. Here one can see the travelled distances of the surface and one sub-surface simulation. The angle is calculated element-wise with the arc-tangent

$$\Theta = \arctan((y_2 - y_1)/(x_2 - x_1)) \quad (6)$$

where y_2 is the latitude of the particle position at each time step, and y_1 is the latitude of the initial position. Likewise, x_2 is the longitude of the particle position at each time step and x_1 is the longitude of the initial position. To calculate the distance on a sphere with latitudes and longitudes, the Haversine formula is applied. It gives the great-circle distance between two

points on a spherical mesh and is defined as

$$d = 2r \arcsin \left\{ \sqrt{\sin^2\left(\frac{y_1 - y_2}{2}\right) + \cos(y_1) \cdot \cos(y_2) \cdot \sin^2\left(\frac{x_1 - x_2}{2}\right)} \right\} \quad (7)$$

where r is the Earth's radius with approximately 6371 km, and x_1, x_2, y_1 , and y_2 are defined likewise (6).

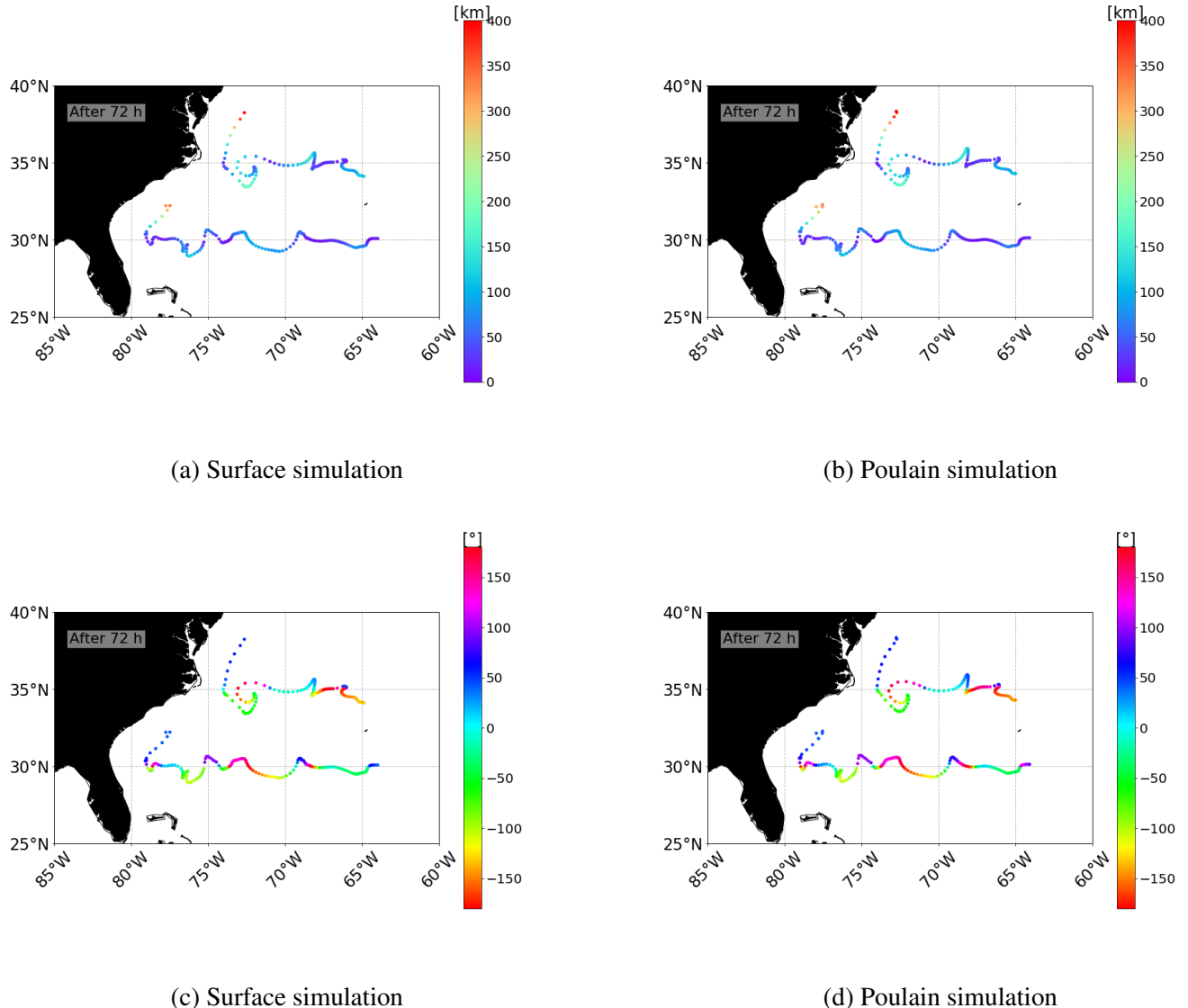


Figure 3: Travelled distances (a, b) and change in angles (c, d) of 270 particles after 3 days. Particles are released simultaneously from two lines: (1) 35° N and 65° - 75° W; (2) 3° N and 65° - 80° W.

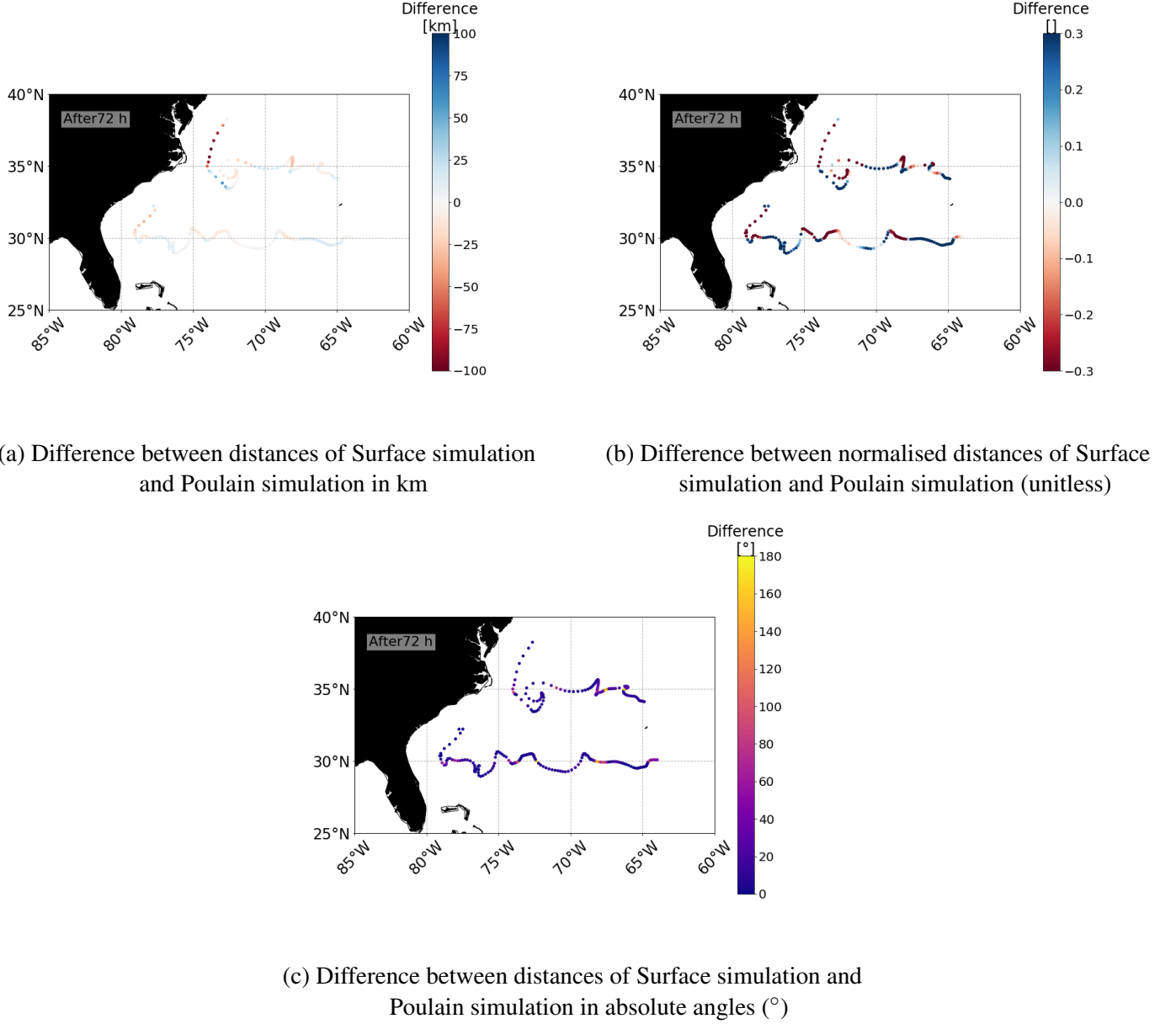


Figure 4: Differences in distances (a, b) and angles (c) after 3 days. The markers represent the particle positions of the surface simulation after three days, and the colorbar shows the difference of surface and sub-surface simulation. In (a, b) positive values indicate larger travelled distances of surface particles than sub-surface particles and vice versa. In (c) a change of direction is represented by the absolute difference between the angles of surface and sub-surface simulations (figure 3 c, d).

As the distances of the particle positions from the initial position are increasing with each time step, the distances are normalised (Min-Max feature scaling) for better comparability with

$$\text{normalised distance} = \frac{x - x_{min}}{x_{max} - x_{min}}. \quad (8)$$

Here x is the distance of the particle position from the particles initial position for one time step.

x_{min} is the smallest distance from one particle to its initial position over the entire set at one time step. Likewise, x_{max} is the largest distance from one particle to its initial position over the entire set at one time step. To analyse the difference of the sub-surface and surface simulations, the calculated distances (7) and angles (6) are subtracted from each other (Figure 4). Precisely, the distances of a sub-surface simulation are subtracted from the surface simulation. The difference of the angles is calculated as absolute value, hence the output ranges from 0° - 180° .

Then, in order to analyse the ocean conditions as drivers for the differences in distances of surface and sub-surface trajectories, the Pearson correlation r of the NEMO variables mixed layer depth (MLD) [m], wind stress τ [Pa], wind speed [m/s], and SSH [m] is calculated point-wise by applying the function of the SciPy collection, a Python-based ecosystem (Jones, Oliphant, Peterson, et al. 2001).

$$r = \frac{\sum(x - m_x)(y - m_y)}{\sqrt{\sum(x - m_x)^2 \sum(y - m_y)^2}} \quad (9)$$

Before computing the correlation it is necessary to change the output of the simulation from a Lagrangian frame of reference into a Eulerian frame of reference, since the NEMO variables are provided on a fixed mesh. Here I calculate the mean of distances from the initial position and changes in directions for each grid cell of a $0.25^\circ \times 0.25^\circ$ resolution meshgrid. Hence, for each grid cell those particles are considered which fall into that grid cell at the given time step. These calculation are performed for all time steps, but in this thesis only the change after 3 days is discussed in detail. The NEMO variables are provided as ORCA grid with a $0.25^\circ \times 0.25^\circ$ resolution, too.

5 Results

5.1 Simulations

The particle depths differ after a three days run of the scenarios 'Poulain' and 'Kukulka'. After the simulation 'Poulain' particles reach depths up to 1000 m (Figure 5), whereas the 'Kukulka' scenario leads to a maximum depth of about 100 m (Figure 6). The particle distribution with depth remains nearly constant over the entire simulation time for both scenarios (Figure 5, 6). Even though this thesis focuses on the first three days, one can see that the distribution over depth remains nearly constant exceeding this time frame. The spatial distribution of vertical mixing matches with the distribution of wind stress τ (Figure 7, 12), since wind stress τ is defined as forcing the vertical mixing of the particles in the custom kernel of the simulations.

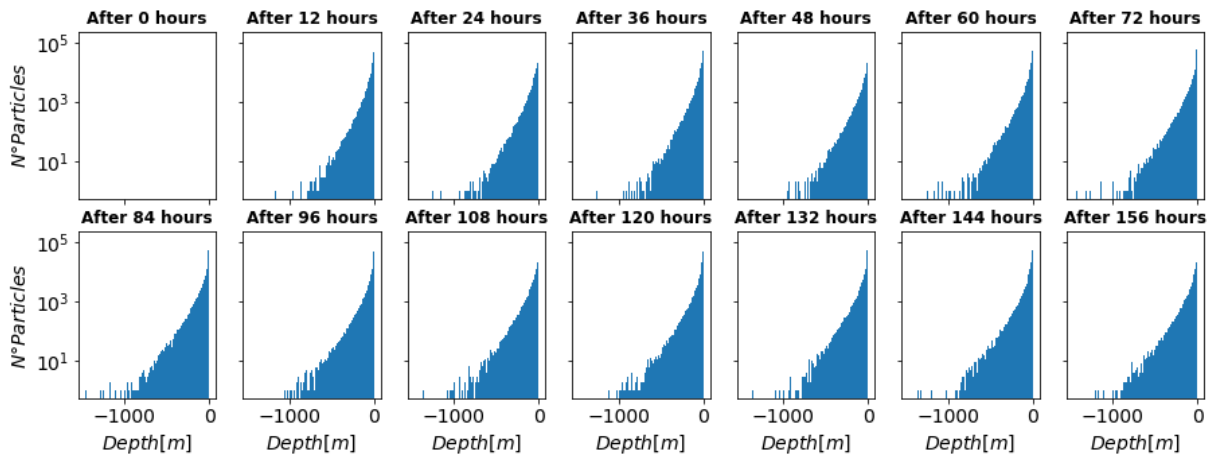


Figure 5: Histogram of particle distribution over depth for simulation 'Poulain'

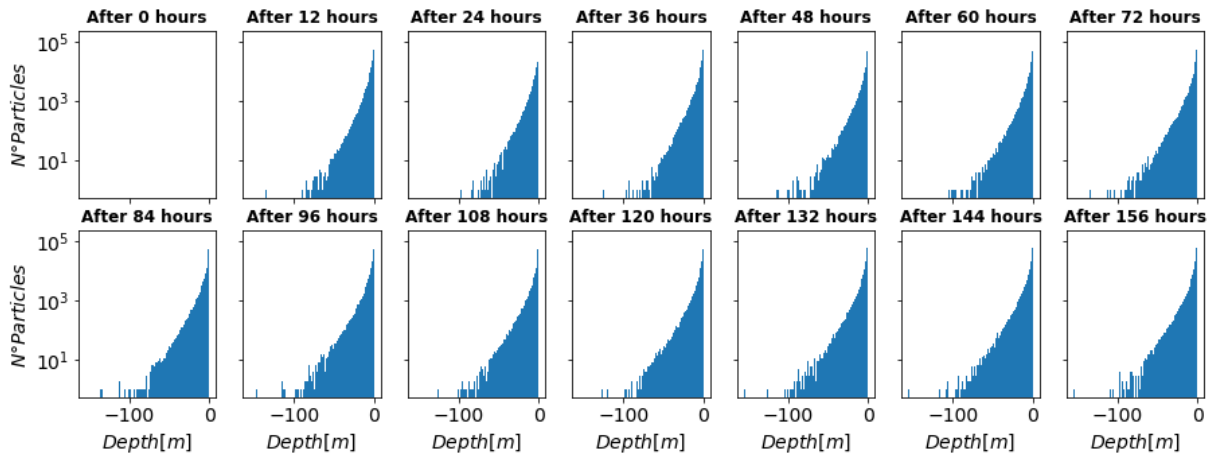


Figure 6: Histogram of particle distribution over depth for simulation 'Kukulka'

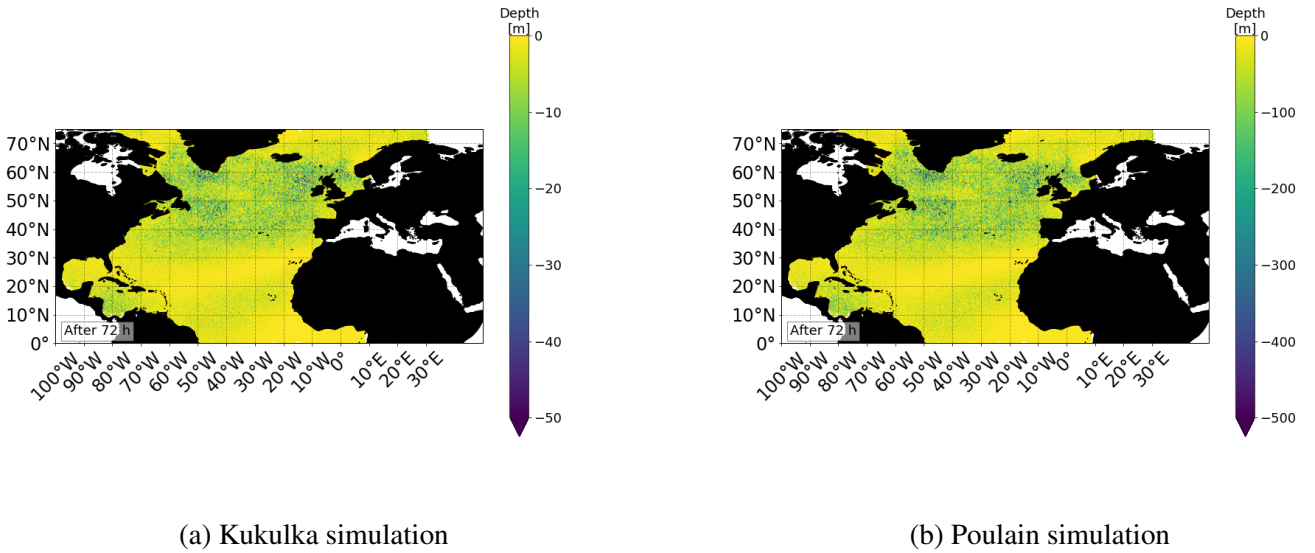


Figure 7: Particle Depths (m) after a simulation run of 3 days. Note the different depth scales of the Kukulka (a) and Poulain (b) simulation.

5.2 Post-Processing

The differences of surface and sub-surface distances of the particles from the initial position after three days show some variation between the Kukulka and the Poulain simulations (Figure 8). The spatial distribution of the differences is very similar, but the magnitude of differences diverges clearly (Figure 8). There are certain areas which show greater covered particle distances of the surface simulation than of the sub-surface simulations (marked in blue) and vice versa (marked in red) (Figure 8). The Gulf Stream shows a noticeable high amount of (red) negative differences, which means that particles of the sub-surface simulations covered a larger great-circle distance, from the initial position to the final position after three days, than the surface simulations. However, there are positive differences in the Gulf Stream, too. The lower latitudes with the North Equatorial Current (NEC, 10° - 20° N), and its Counter Current (NECC, 3° - 10° N) are structured by adjacent negative and positive differences in distances, whereas negative differences are most distinct around 10° N. The Labrador Sea, especially the Labrador current (LC), and the Baffin Island Current (BIC) show distinctively more positive differences in distances. This also accounts for the Caribbean Sea. Overall, the shape of the differences in distances indicates the eddy structure of the currents in the North Atlantic. The computed distances and angles for the single simulations, illustrated as maps, can be found in the annexes (Figures 20, 21, 22).

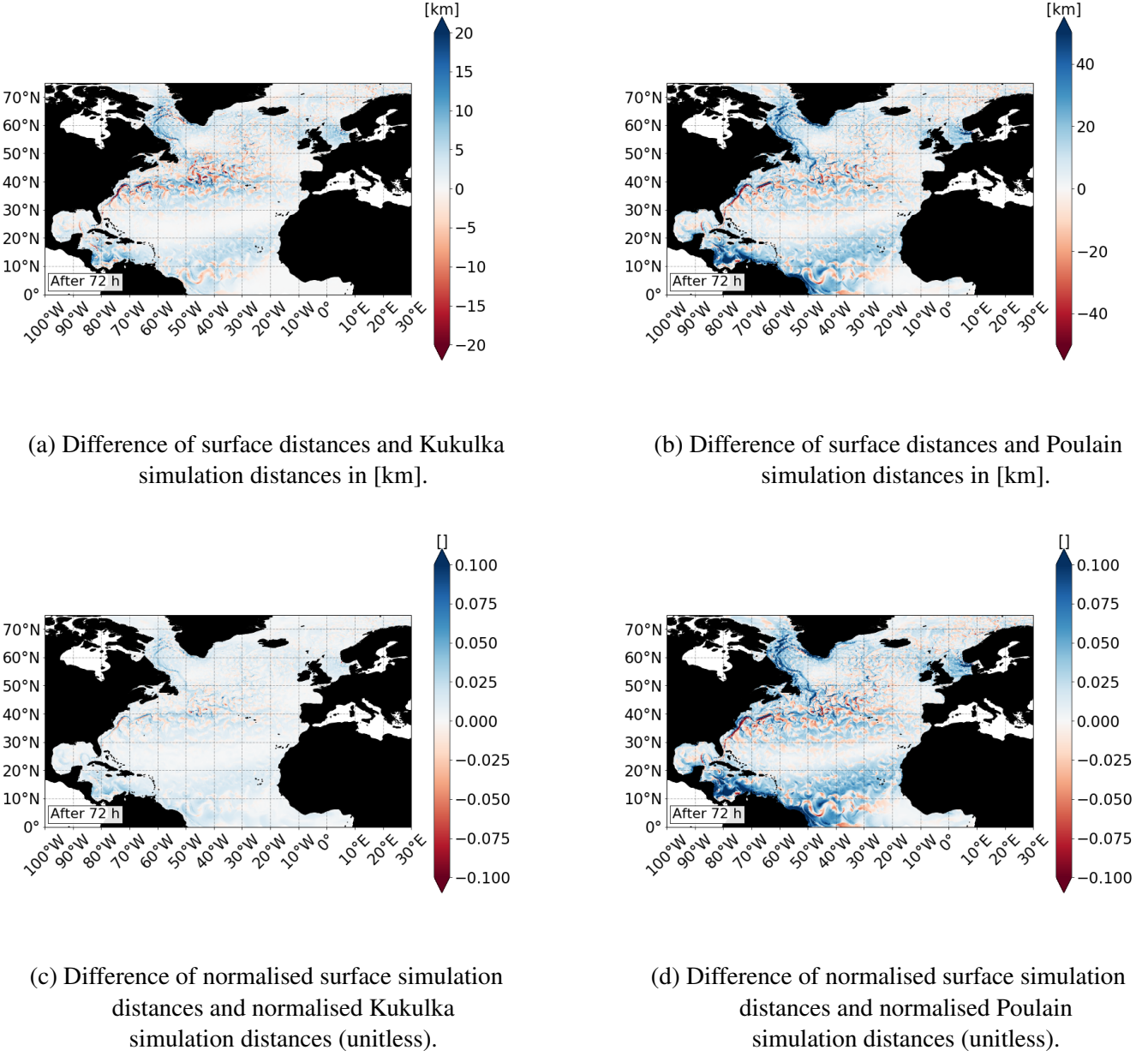


Figure 8: Differences of surface and sub-surface distances after 3 days for the North Atlantic. Positive distances indicate that surface distances are larger than sub-surface distances and vice versa. Note the different scales of (a, b).

Compared to the differences in distances, the absolute differences in direction, i.e. the absolute change of the angles from the initial position to the position after three days, shows a less distinctive distribution (Figure 11). However, the changes in direction are still more distinctive for the Poulain simulation than for the Kukulka simulation.

In figures 9 and 10 the evolution of the travelled particle distances among depth is shown. It demonstrates, that the covered distances at shallower depth are larger than at greater depths. However, the majority of particles is located near the surface and covers relatively low distances.

This is due to two conditions: The spatial distribution of strong wind stress τ , which forces the particles to be mixed downwards in this scenario, covers only parts of the North Atlantic (Figure 12 a). Thus, the majority of the particles stays at the surface. Furthermore, relatively large distances travelled by the particles occur only along strong ocean currents (Figures 20 - 22). The major difference of Kukulka and Poulain mixing is determined by the maximum particle depth.

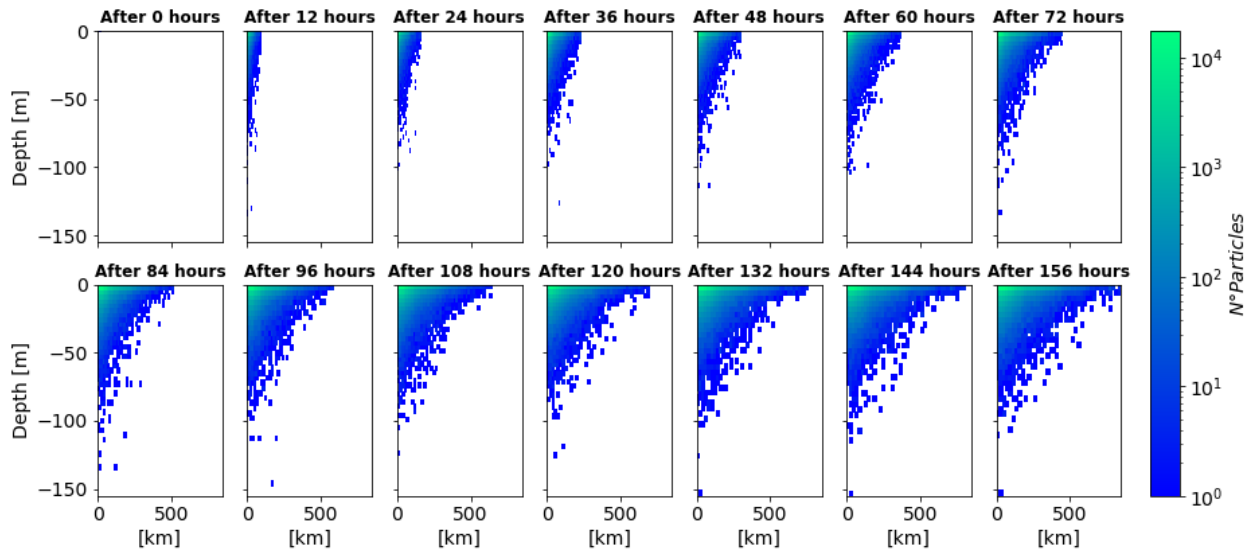


Figure 9: 2D Histogram of distance in [km] versus depth [m] - Kukulka simulation

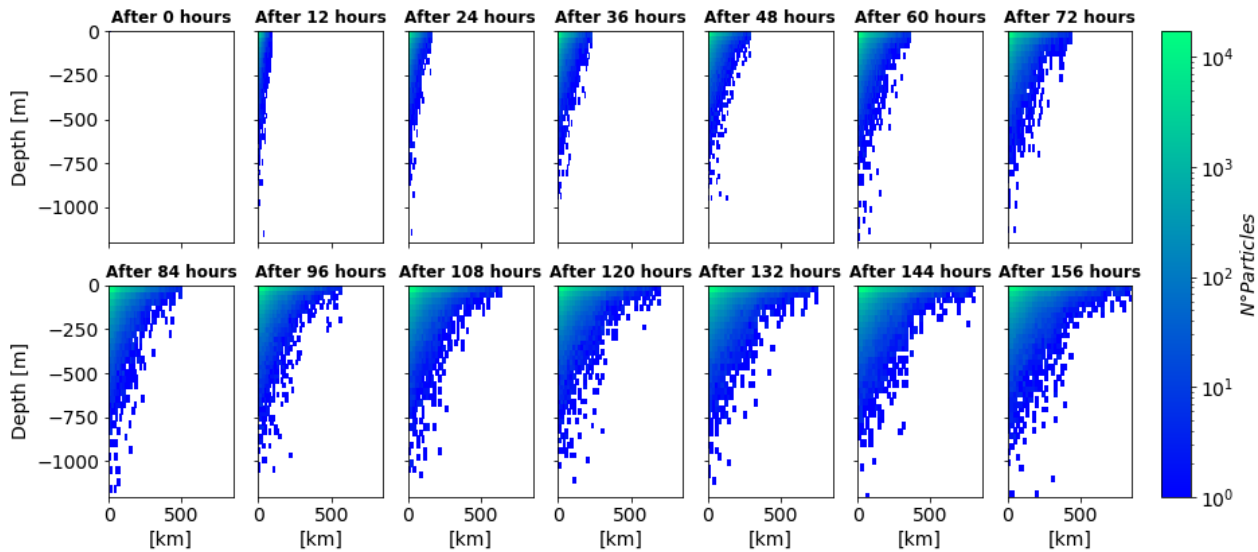
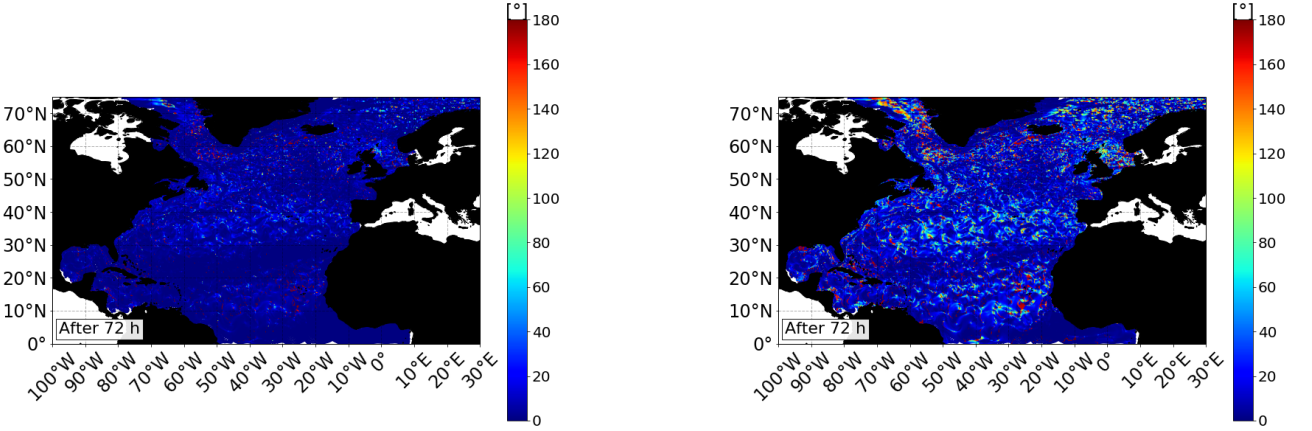


Figure 10: 2D Histogram of distance in [km] versus depth [m] - Poulain simulation



(a) Difference of surface directions and Kukulka simulation directions in absolute values [°].

(b) Difference of surface directions and Poulain simulation directions in absolute values [°].

Figure 11: Differences of surface and sub-surface directions after 3 days for the North Atlantic. Note that the differences are in absolute values, hence they only indicate the absolute change of direction, but not the orientation.

5.2.1 Correlations

Overall, the Pearson correlation r is relatively low for all combinations of NEMO variables and differences of distances of both simulation (Figures 13 - 17 & 23 - 27). I perform the correlation of the differences between the surface and sub-surface distances and the NEMO variables, because the differences between the distances show a stronger pattern than the changes in directions. The NEMO variables are presented in figure 12. As the variables are provided as 5-day mean, they do not change with time. Since the vertical mixing is forced by wind stress τ , I investigate if the magnitude of τ is correlated with the differences between surface and sub-surface distances. Additionally to wind stress, I perform the correlation with the wind speed, because the wind stress vector can deviate significantly from the wind speed direction, and the wind stress direction affects significantly the wind stress magnitude (Sheng et al. 2018). Then, the MLD is taken into consideration as it is dominated by wind mixing among other processes such as heat exchanges at the sea-air interface. Finally, SSH is investigated as it gives insight into the mesoscale eddy structures, and these eddies structures seem to have the capability of trapping particles (Figure 4). Since the two-dimensional histograms of the NEMO variables and the differences in distances (sub-surface distances substracted from surface distances) do only show small differences between the Poulain and Kukulka simulation, only the outputs for the Poulain simulation are shown here (Figures 13 - 17). The plots for the Kukulka simulation can be found in the annexes, and outstanding differences between the simulations are discussed in this chapter and the discussion.

1. North Atlantic (30°E - 97°W & 0 - 75°N)

The results of the Kukulka and the Poulain simulation against the NEMO variables for the North Atlantic show many features in common, but also some differences (Figures 23, 13). With increasing wind speed and stress the range of differences in distances increases (Figures 23 a, b & 13 a, b). With increasing MLD until about 100 - 150 m, the range of differences tends to increase, but the majority of particles is centred close to 0 [] difference (Figures 23 c & 13 c). However, in the results of the Poulain simulation the differences are likely more positive than negative until a MLD of about 50m. The distribution of the differences against SSH appears to be nearly random (Figures 23 d & 13 d).

2. Gulf Stream (70 - 80°W & 30 - 40°N)

Likewise, as for the whole North Atlantic, the range of differences in distances increases with increasing wind speed and stress in the section of the Gulf Stream (Figures 24 a, b & 14 a, b). At MLDs of about 100 - 150 m the highest range of differences occurs and the differences are showing slightly lower values with increasing MLD. This trend tends to be stronger for the Poulain simulation than for the Kukulka simulation (Figures 24 c & 14 c). Moreover, the differences in distances against SSH show a pattern: With negative SSH, the amount of positive differences increases, whereas with positive SSH the amount of negative differences increases (Figures 24 d, 14 d).

3. Labrador Sea (50 - 64°W & 55 - 55°N)

The relation of the wind stress τ and speed and the differences in distances does not indicate any particular pattern, besides that there are stronger winds over the Labrador sea than over the Gulf stream section (Figures 12 a, b & 25 a, b & 15 a, b). Then, with increasing MLD the differences decrease and with decreasing MLD the range of differences increases and is shifted towards positive values (Figures 25 c, 15 c). This shift is intensified in the Poulain simulation.

4. North Equatorial Counter Current (NECC) (30 - 50°W & 0 - 10°N)

Overall, there is a higher amount of positive than negative differences of distances for the NECC section (Figure 26). However, this rate is diminished in case of the Poulain simulation (Figure 16). Furthermore, the surface tends to be faster than the sub-surface with increasing MLD (Figures 26, 16). But with the addition that this relation is very weak.

5. Center (30 - 60°W & 30 - 60°N)

Again, the range of differences in distances increases with increasing wind speed and stress for both simulations (27 a, b & 17 a, b). Here, the range of differences is relatively

larger in case of the Poulain simulation. The differences against MLD does not show such a pattern (Figure 27 c, 17 c).

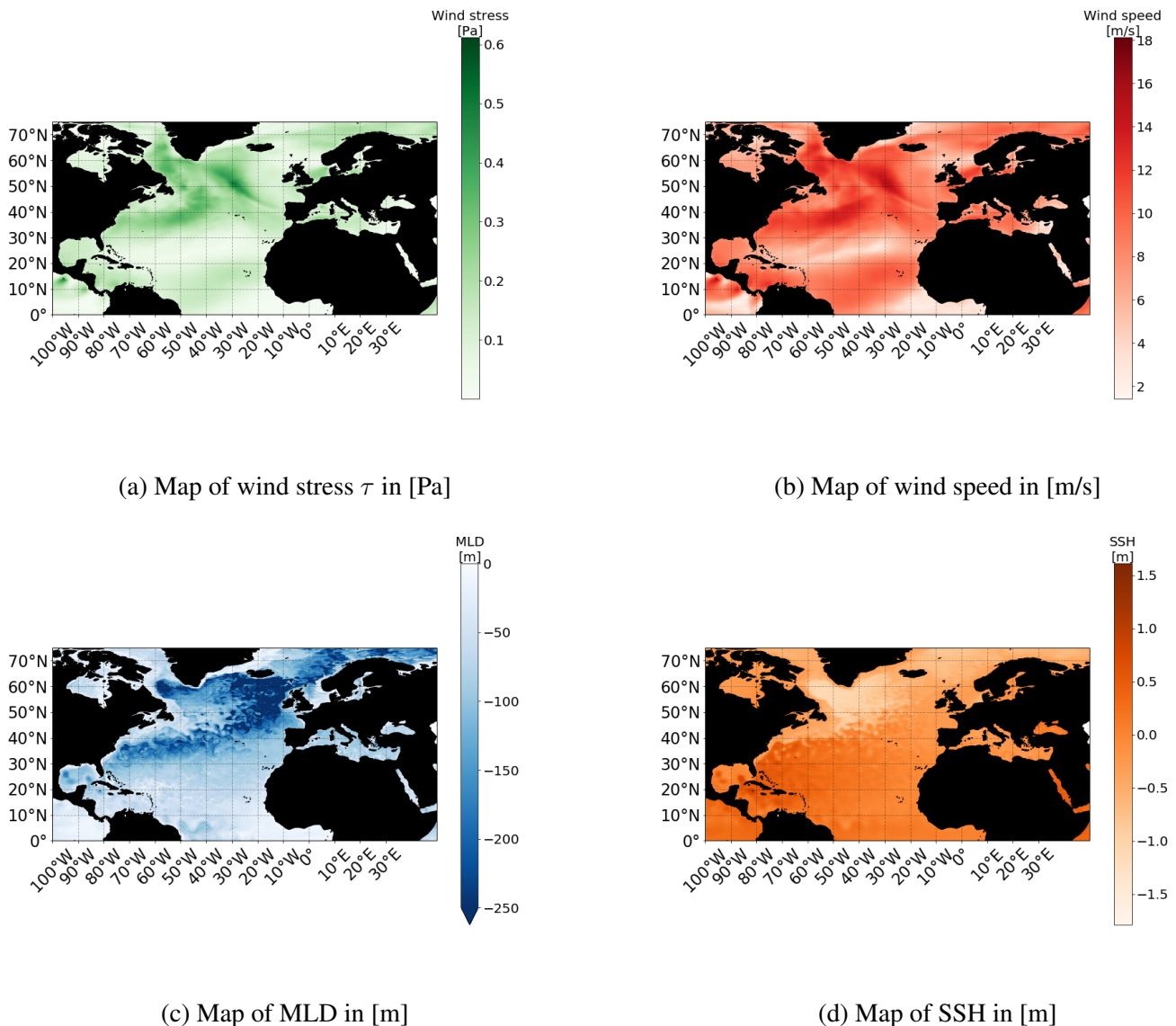


Figure 12: Various NEMO variables: 5-day means simultaneous with PARCELS simulations (compare table 1).

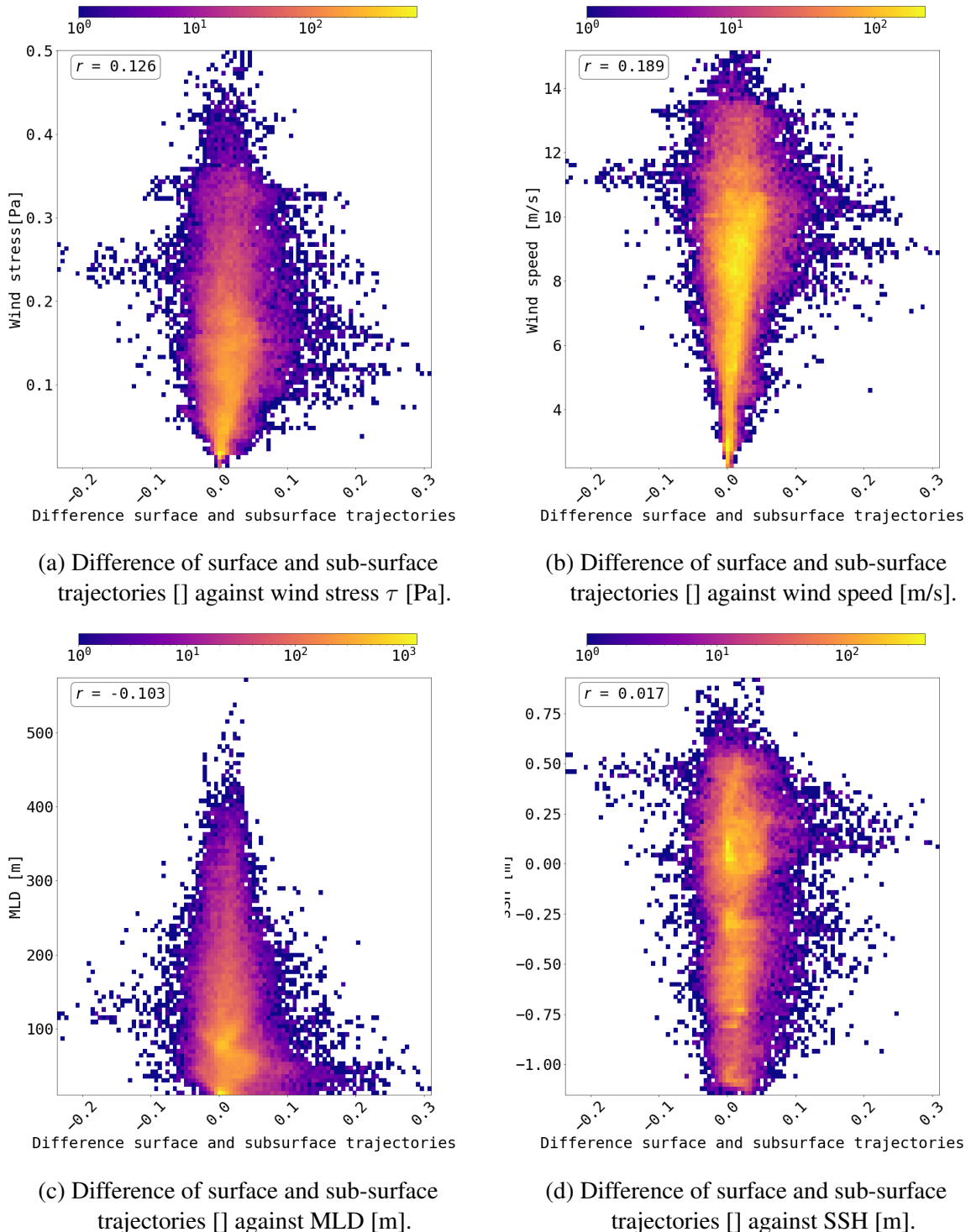


Figure 13: Poulain mixing - North-Atlantic: Two-dimensional histograms of surface distances minus sub-surface distances [m] against various NEMO variables. Additionally, the Pearson correlation r is calculated.

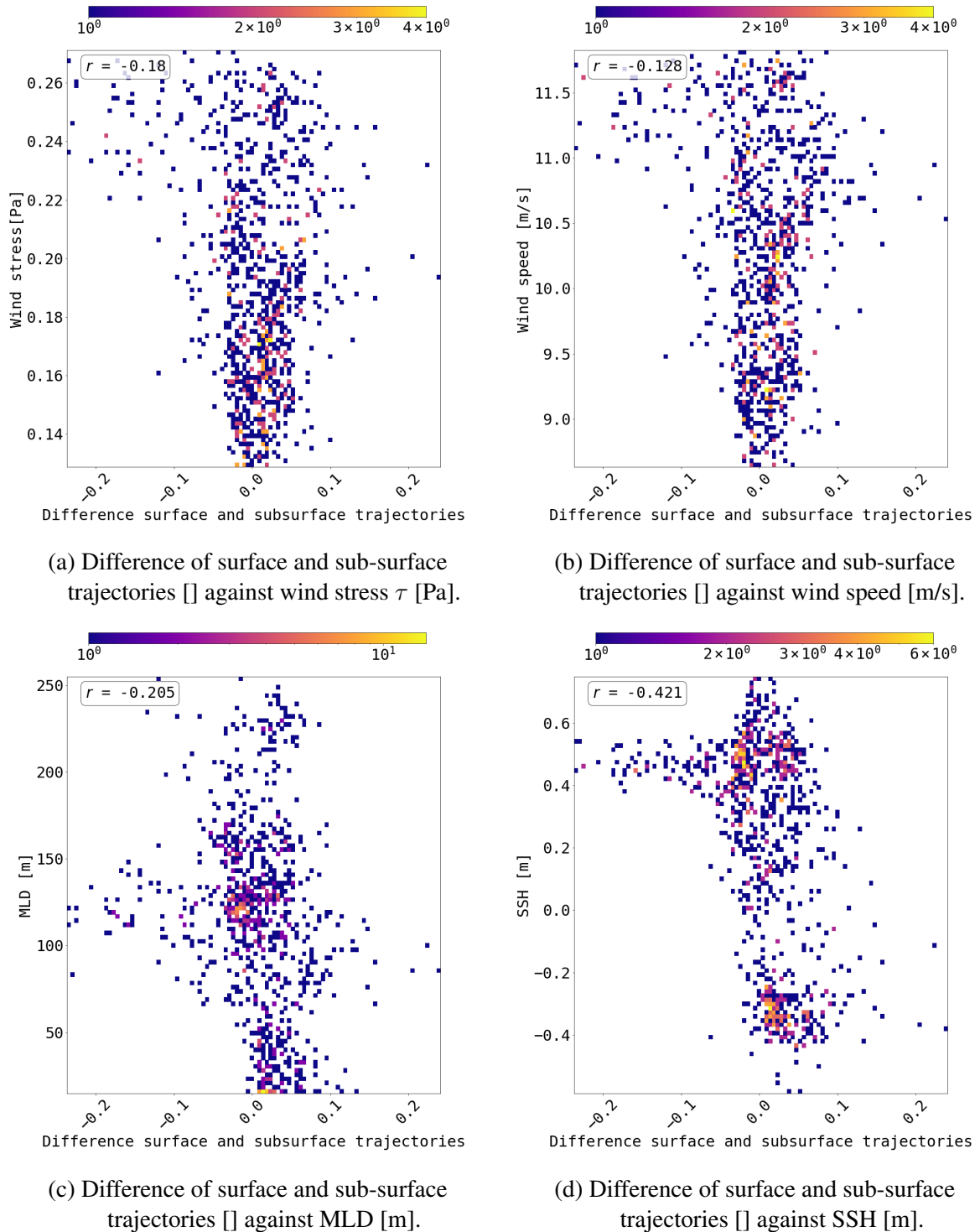


Figure 14: Poulain mixing - Gulf stream: Two-dimensional histograms of surface distances minus sub-surface distances [] against various NEMO variables. Additionally, the Pearson correlation r is calculated.

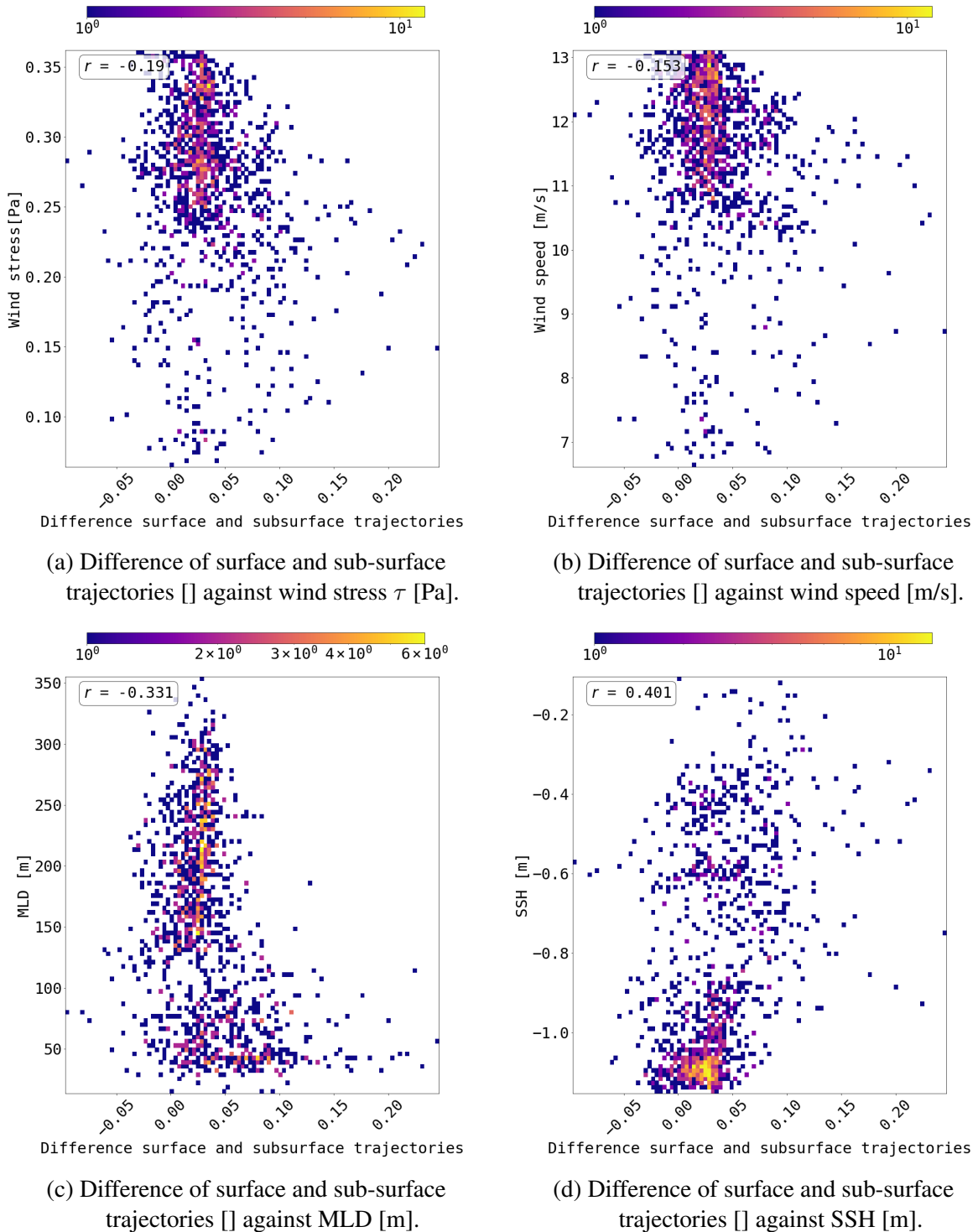


Figure 15: Poulain mixing - Labrador sea: Two-dimensional histograms of surface distances minus sub-surface distances [] against various NEMO variables. Additionally, the Pearson correlation r is calculated.

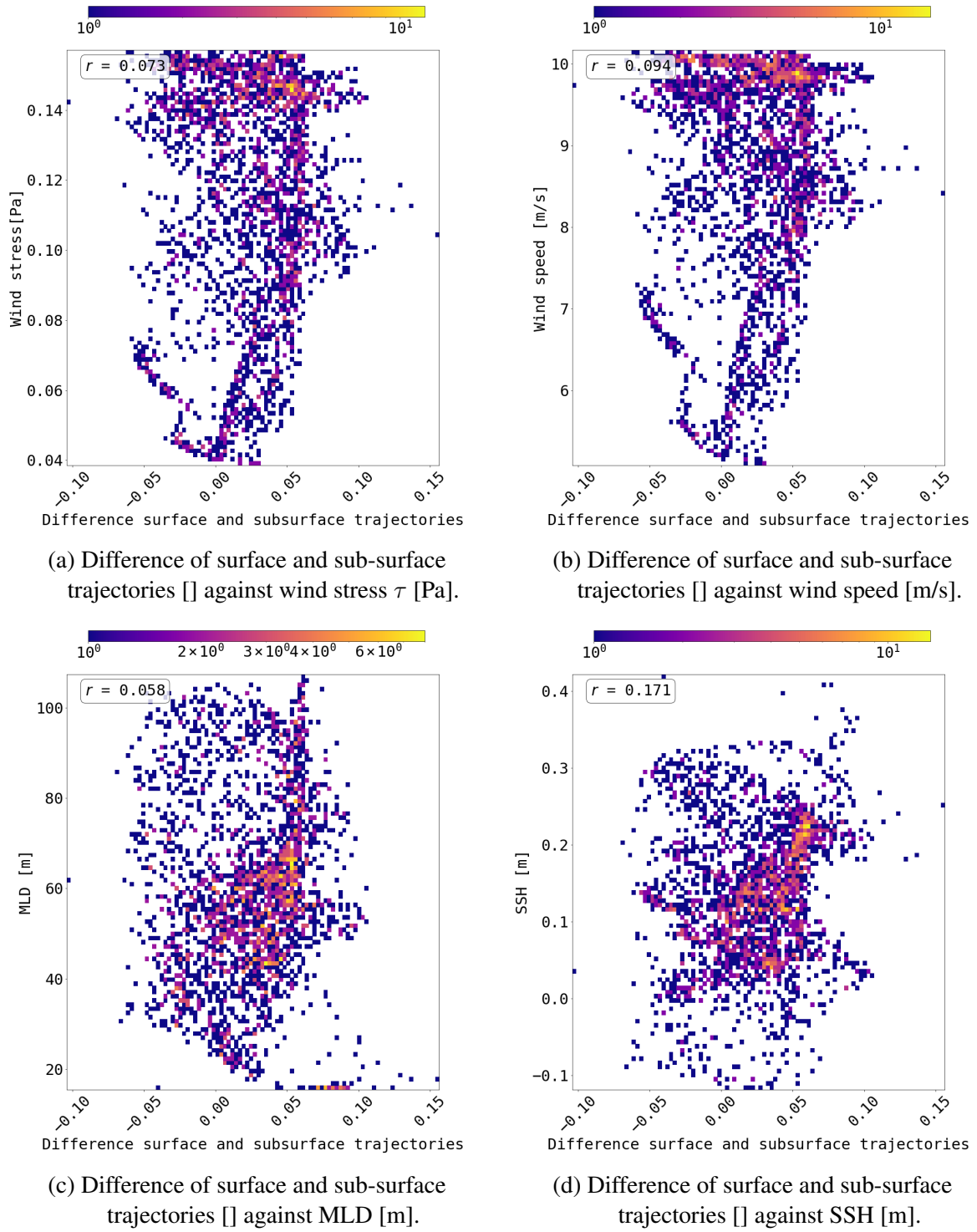


Figure 16: Poulain mixing - Equatorial current: Two-dimensional histograms of surface distances minus sub-surface distances [m] against various NEMO variables. Additionally, the Pearson correlation r is calculated.

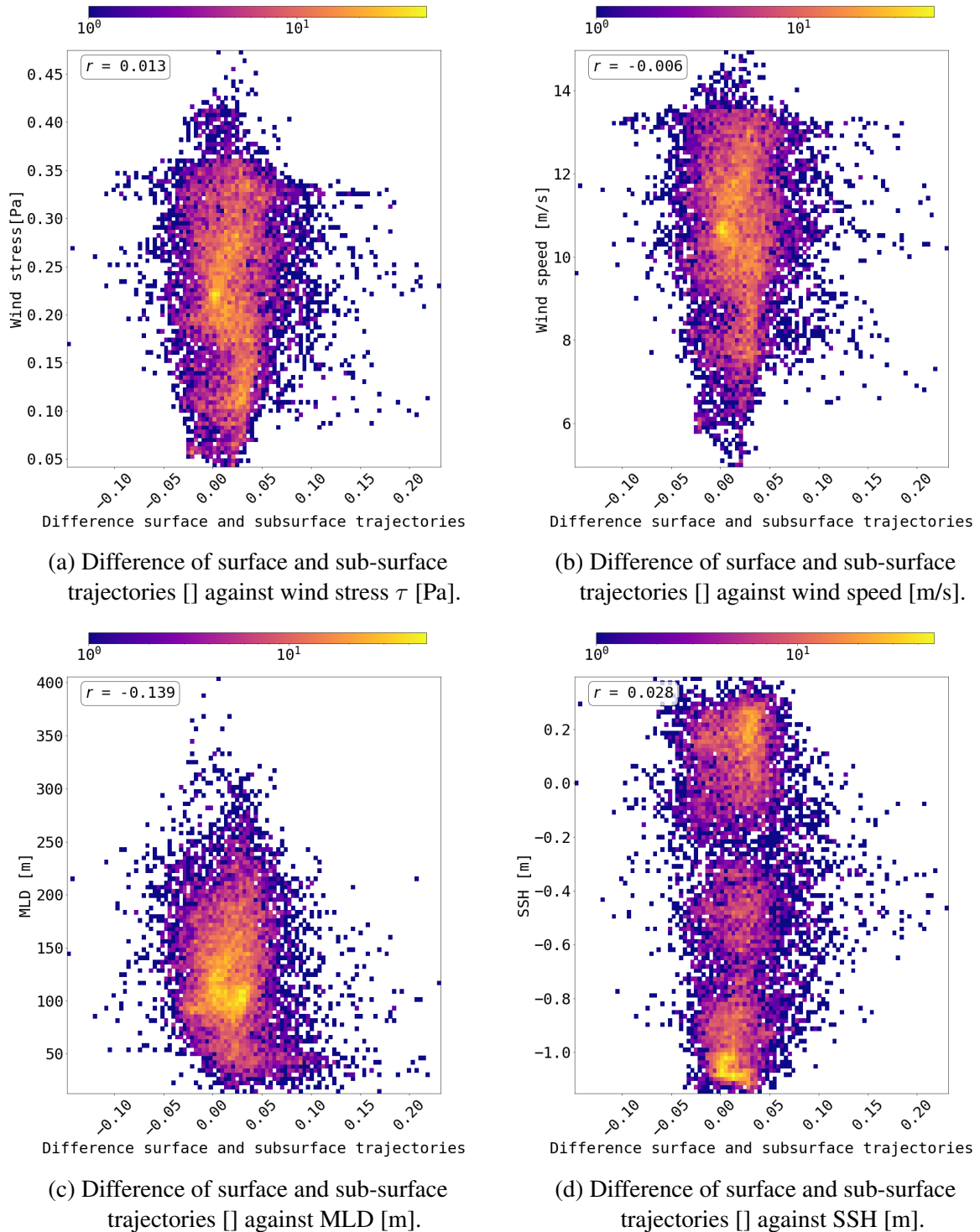


Figure 17: Poulain mixing - Center: Two-dimensional histograms of surface distances minus sub-surface distances [] against various NEMO variables. Additionally, the Pearson correlation r is calculated.

6 Discussion

The North Atlantic is as very well studied but complex structure of various turbulent flows. The flow structure is determined by a mid-latitude basin-wide gyre and the Gulf Stream, the northward western boundary current. Moreover, it is structured by a subpolar gyre with the Labrador Current, and finally the equatorial current system with the North Equatorial Current and the North Equatorial Counter Current. Therefore, the comparison of the whole North Atlantic against the various NEMO parameters is not very precise but rather providing some initial concepts (Figure 23, 13).

That the range of differences in distances increases with increasing MLD (until a MLD of 100 - 150 m) towards positive and negative differences, indicates two different aspects of the chaotic structure: (1) As described by the Ekman-spiral, sub-surface currents decrease in velocity with increasing depth. Hence, surface currents would be faster and cover larger distances than sub-surface currents. Even though the Ekman-Spiral is an idealised description of the actual process determining the ocean surface layer, and only observed under ice (Hunkins 1966), Ekman-transport is observed as determining process in the global ocean. (2) Particles carried by surface currents can be trapped in eddies, and if deeper situated sub-surface particles are not trapped in eddies, they could cover larger distances than the surface particles. Hence, it would be interesting to further investigate this hypothesis with applying the Nencioli algorithm as in Cetina-Heredia et al. (2019). It can be used to analyse the eddy depth, but only for a straight depth extent of the eddy. With the diagnosis of the eddy depth it would be possible to identify whether surface particles are trapped in eddies, but sub-surface particles are not. Cetina-Heredia et al. (2019) quantified the time that eddies retain water and the substances and properties carried by these eddies. Even though their research invested eddies along the southeast coast of Australia, eddies occur globally. They found that the retention time varies from a few days to a year, but a peak occurs around 24 to 27 days. Moreover, elongated eddies tend to leak entrained water and the carried substances such as MP, hence the eddy eccentricity is an indicator of the water exchange from the eddy with its surrounding.

Moreover, it is shown that the Poulain simulation leads to rather greater travelled surface distances than sub-surface distances until a MLD of 50 m (Figure 13 c), which could be caused by the great depths the particles reach in the Poulain simulation, with a maximum of about 1000 m. Thus, one could hypothesise that, with a MLD of 50 m, particles could reach depth exceeding the MLD, where current velocities could be rather low. However, as this histogram accounts for the whole North Atlantic, its needs further investigation.

The greatest MLDs are present along the Gulf Stream, the Labrador Sea, and a vast area north of Iceland (Figure 12 c), whereas co-located noticeable differences of distances only appear along the Gulf Stream, but not in the distinctive areas with great MLDs in the Labrador Sea or North of Iceland (Figure 8). Moreover, these not co-located areas with great MLDs, lack in the

potential of carrying surface or sub-surface particles along large horizontal distances (Figure 20, 21, 22). Thus, the differences between these distances are rather small, too.

The decrease of wind stress τ is calculated from the wind speed with a drag coefficient. This means, that the wind stress τ is the vertical transfer of the horizontal momentum from the atmosphere to the ocean. Thus, the shape of the two-dimensional histograms of wind stress τ and wind speed against the difference of distances is similar, but not equal (Figures 23 a, b & 13 a, b). With increasing wind speed and stress τ , the range of differences increases. As wind stress τ is the factor forcing the particles to be mixed downwards, the sub-surface particles are reaching greater depths with increasing wind stress and their pathways are determined by either Ekman-transport or exceeding the Ekman-depth. Both the changes in conditions would lead to varying directions and distances. Hence, the range of differences increases. The differences of distances against the SSH are almost evenly distributed (Figures 23, 13).

There is a pattern of the differences between distances against the SHH in case of the Gulf Stream (Figure 24 d, 14 d). Here, the correlation is stronger for the Poulain simulation than for the Kukulka simulation with $r = -0.421$. Thus, with increasing SSH the differences in distances decrease, i.e. the surface particles cover smaller distances than the sub-surface particles. However, this pattern is not shown by the majority of particles.

The Sargasso Sea is covered by greater SHH than the shelf water (Figure 12 c). Moreover, there are SSH structures which indicate mesoscale eddies. The unstable meandering of the Gulf Stream leads to a high amount of eddies. Within the section of 70 - 80 °W and 30 - 40 °N, rings of lower SSH than the adjacent water occur which indicate cold core rings transporting cold water westwards. The sharp line of changing SSH in the section 70 - 80 °W and 30 - 40 °N (Figure 12 d) coincides with the red line of negative differences in distances (Figure 8). The velocity of the Gulf Stream is fastest at the surface, but this maximum can cover the upper 200 m. The depth of the Gulf stream is about 1200 m. As the Gulf Stream generates eddies, the smaller surface distances than sub-surface distances presented as a distinctive red line in figure 8 could be due to eddy-trapped particles in the surface flow. However, as eddies can propagate through depths, this hypothesis needs further investigation.

Moreover, the negative correlation of differences in distances and SSH indicates that the red line of negative distances is situated at the outer edge of the sharp barrier in SSH mentioned before. As observed for the whole North Atlantic and discussed before, the range of differences increases with increasing wind speed and stress τ for the Gulf Stream in particular, too (Figures 24 a,b & 14 a,b). Again, as wind stress τ forces the particles to sink in this model, and particles likely experience a change of direction and velocity with depth, the deviation from the surface trajectories increases.

In case of the Labrador Sea section, the range of differences in distances does not increase with increasing wind stress τ or wind speed (Figure 25 a, b & 15 a, b). As wind stress forces

downward mixing, this means that increasing downward mixing does not directly lead to deviations of covered surface and sub-surface distances. However, with increasing MLD, the range of differences in distances decreases (Figures 25 c, 15 c). And furthermore, it shifts towards positive differences with decreasing MLD for the Poulain simulation in particular. This means, that covered surface distances tend to be greater than sub-surface distances in areas with a relatively low MLD. In figure 8 one can see that the Labrador Sea is determined by greater surface distances than sub-surface distances. By comparison with figure 12 c, it becomes clear that the differences occur where the MLD is relatively low. Moreover, the blue line of differences in figure 8 surrounds the areas of high MLD values (Figure 12 c). As the Labrador Current is a strong surface current with decreasing velocities through depth (ref), the larger covered surface distances could be forced by this current structure.

As the Coriolis effect weakens towards the equator, the section representing the NACC from 0 - 10°N - 10 and 30 - 50 °W, is determined by a strong seasonal signal which is due to seasonal changes of wind forcing. For that reason, the westward propagating NACC is weakest during later winter and strongest during austral summer months. Hence, the time span of one week in January, as investigated in this thesis, does not cover the maximum potential of this area, but rather weak currents. However, this section is still determined by a noticeable structure of differences in distances, which are spatially distributed with a high similarity to the boundary of different MLDs (Figures 8, 12 d). Negative distances, i.e. relatively large covered subsurface distances, appear at the edge of meandering eddy-structures which are indicated through differences of MLDs. Moreover and again, the range of differences in distances increases with increasing wind stress τ and speed (Figures 26 a, b & 16 a, b). Overall, the range of differences is greater for the Poulain simulation than for the Kukulka simulation, because particles are mixed deeper in the first one.

Finally, the section with the indices 30 - 60 ° N and 30 - 60 ° W also indicates an increasing range of differences in distances with increasing wind forces, and moreover a higher range due to the Poulain mixing than the Kukulka mixing (Figures 26 a, b & 16 a, b). Again, in case of the Poulain simulation, the surface particles tend to travel larger distances than sub-surface particles in regions of relatively low MLD until about 50 m (Figure 17 c). This does not account for the Kukulka simulation (Figure 27 c). The majority of particles in the Kukulka simulation does not exceed a depth of 50 m, whereas the majority of particles in the Poulain simulation likely exceeds a depth of 50 m to about 150 - 200 m (Figures 18, 19).

Windage has a direct impact on surface MP pathways, but not on sub-surface MP-pathways (Chubarenko et al. 2016). However, in this study windage effects on the surface trajectories are not taken into consideration. Surface, as well as sub-surface pathways are forced by the meridional and zonal current velocities from the NEMO dataset only. Hence, effects affecting surface trajectories only are ignored. Another drawback is that wind stress τ is provided as magnitude

in the NEMO dataset, hence the information about the direction is missing and cannot be taken into account within the interpretation of the results.

Moreover, biofouling is not parameterised in this approach. As MP-particles experience biofouling, i.e. a biofilm covering the particle, they experience a loss of buoyancy (Ryan 2015, Kooi et al. 2017). This change of behaviour is significantly increased with the settlement of macro-organisms on the particle surface (Kaiser, Kowalski, and Waniek 2017). Moreover, the rate of fouling differs among the different ecosystem of the ocean (e.g. coastal areas vs. open ocean) (Kaiser, Kowalski, and Waniek 2017). Chubarenko et al. (2016) conclude that fouling of MP is linearly dependent on the characteristic length scale of a particle. The smaller the particle, the faster it is fouled up to the water density (Chubarenko et al. 2016, Kooi et al. 2017, Ryan 2015). Hence, particles with an originally lower density than the surrounding water experience an increased sinking rate, and particles with an originally larger density than the surrounding water lose buoyancy and sink. However, Kaiser, Kowalski, and Waniek (2017) dispute that very small particles can be lined up in this linear relation, as the attachment of macro-organisms leads to significant changes in density. M.C. Fazey and Ryan (2016) define the factors influencing the fouling rates as: Season, geographic location, water temperature, nutrient levels, substrate type and the velocity and turbulence of the surrounding water flow. As the experiments performed by Kaiser, Kowalski, and Waniek (2017), Kooi et al. (2017), and Ryan (2015) are exclusively laboratory or harbour experiments, oceanic conditions can only be roughly derived from these outputs. Because of the complexity of this combinations, modelling vertical transport due to biofouling represents a research question which falls out of the scope of the project, although it needs to be discussed as missing parameter leading to changes of vertical movement. Another underestimated biotic factor, influencing the vertical transport of marine MP, is the direct transport by marine organisms such as particle feeders (Choy et al. 2019).

An additional constrain of this research is that the rise velocities are subdivided into two classes only (Kukulka vs. Poulain simulation). Overall, the rise velocities applied in this thesis are relatively low in comparison to the ranges estimated by Kukulka et al. (2012), Reisser et al. (2015), and Poulain et al. (2019). Hence, higher modelled rising velocities would lead to smaller depth of the particles, and eventually to smaller differences of distances of surface and sub-surface trajectories. The empirical model of Kukulka et al. (2012) does not distinguish in between various particle sizes and shapes, but the approach of Poulain et al. (2019) allows to adjust the rising velocity with respect to size and shape. Again, this thesis only investigated the smallest possible rising velocity, which represents a very small, spherical particle. A diversification of these characteristics, based on observed compositions of MP in the North Atlantic, would further increase the accuracy of this approach.

Furthermore, the time frame of this approach leads to a time-shot observation of the ocean conditions. As the physical processes underlay seasonal signals, and moreover interannual signals, this can be considered to be a first step in the investigation of the potential to estimate

three-dimensional flows from two-dimensional products such as SKIM measurements. As the significance of this approach depends on the significance of measurement- and experiment-results, it also depends on further investigation of the behaviour of marine MP, especially its vertical movement.

Another drawback of this study is the assumed constant water density through the whole North Atlantic, but as the MP densities defined in the simulations vary over much larger magnitudes than the water density, this can be neglected.

The final drawback which needs to be mentioned is that the difference of distances and angles is a calculated mean from about 4 trajectories for each grid cell of 0.25° resolution. This step is needed as the Lagrangian output needs to be converted to an Eulerian specification of the field in order to gain a comparability with the NEMO variables. However, this leads to a rather simplified output and reduces the significance. The maximum particle depths of the simulations (Figures 18, 19) also needs to be discussed. As the majority of MP sub-surface sampling studies focus on the upper meter of the surface boundary layer (Kooi et al. 2016), the output of the simulations cannot be confirmed by measurements. However, Poulain et al. (2019) concluded that SMP can be transported downwards to several hundred m depths. To the best of my knowledge there is no research which concluded that buoyant SMP particles can be mixed downwards until 1000 m depth.

7 Conclusion

In four of five investigated areas (including the whole North Atlantic) increasing wind stress, i.e. greater particle depths due to downward mixing, result in larger differences in distances of surface and sub-surface MP-pathways. Here, the Labrador Sea forms an exception. However, the vertical mixing itself does not cause the differences, but the changing physical processes among depth are the causes. As these changes vary among the whole North Atlantic, and even underlay annual and interannual changes, there is not one common answer. And the greatest differences in distances do not co-appear with the greatest particle depths. Moreover, the major differences occur along strong ocean currents, which are forming eddies. Hence, particles can be trapped in eddies and therefore the covered distance decrease. The vast gyres, where marine plastic accumulates, are not characterised by large differences of surface and sub-surface distances of MP-pathways. These areas appear with small differences. However, as the surface velocities in the gyres are relatively low, the accuracy of SKIM measurements also decreases. The research questions can be answered as follows: (1) There is a significant difference of surface and sub-surface MP-pathways in the North-Atlantic. (2) The driving forces leading to the differences depend on the investigated area, there is not one common answer to this. However, the differences clearly follow a structure, namely they increase along strong ocean currents,

which are part of the meridional overturning circulation. (3) In order to profoundly estimate the potential of using two-dimensional products such as SKIM measurements, further simulations, with varying rising velocities and annual and interannual time-series would be promising. As this study is only a short time frame of one week, the interannual and annual changes of differences in distances and directions cannot be observed. Finally, a neural network, e.g. the Multi-layer Perceptron regressor, bares the potential to develop a parameterization of SKIM measurements and sub-surface flows.

References

- Andrady, Anthony. 2011. "Microplastics in the marine environment". *Marine pollution bulletin* 62 (): 1596–605. doi:10.1016/j.marpolbul.2011.05.030.
- Ardhuin, Fabrice, et al. 2019. "SKIM, a candidate satellite mission exploring global ocean currents and waves". *Frontiers in Marine Science* (). doi:10.3389/fmars.2019.00209.
- Ardhuin, F., et al. 2018. "Measuring currents, ice drift, and waves from space: the Sea surface KInematics Multiscale monitoring (SKIM) concept". *Ocean Science* 14 (3): 337–354. doi:10.5194/os-14-337-2018.
- Cai, Liqi, et al. 2018. "Observation of the degradation of three types of plastic pellets exposed to UV irradiation in three different environments". *Science of The Total Environment* 628-629:740–747. doi:<https://doi.org/10.1016/j.scitotenv.2018.02.079>.
- Cetina-Heredia, Paulina, et al. 2019. "Retention and Leakage of Water by Mesoscale Eddies in the East Australian Current System". *Journal of Geophysical Research: Oceans* 124 (4): 2485–2500. doi:10.1029/2018JC014482.
- Choy, Anela, et al. 2019. "The vertical distribution and biological transport of marine microplastics across the epipelagic and mesopelagic water column". *Scientific Reports* 9 (): 7843. doi:10.1038/s41598-019-44117-2.
- Chubarenko, Irina, et al. 2016. "On some physical and dynamical properties of microplastic particles in marine environment". *Marine Pollution Bulletin* 108 (). doi:10.1016/j.marpolbul.2016.04.048.
- Craik, A. D. D. 2005. "George Gabriel Stokes on Water Wave Theory". *ANNUAL REVIEW OF FLUID MECHANICS* 37:23–42.
- Delandmeter, P., and E. Van Sebille. 2019. "The Parcels v2.0 Lagrangian framework: new field interpolation schemes". *Geoscientific Model Development Discussions* 2019:1–24. doi:10.5194/gmd-2018-339.
- Enders, Kristina, et al. 2015. "Abundance, size and polymer composition of marine microplastics $\geq 10 \mu\text{m}$ in the Atlantic Ocean and their modelled vertical distribution". *Marine pollution bulletin* 100 (). doi:10.1016/j.marpolbul.2015.09.027.
- Hardesty, Britta D., et al. 2017. "Using Numerical Model Simulations to Improve the Understanding of Micro-plastic Distribution and Pathways in the Marine Environment". *Frontiers in Marine Science* 4:30. doi:10.3389/fmars.2017.00030.
- Hunkins, Kenneth. 1966. "Ekman drift currents in the Arctic Ocean". *Deep Sea Research and Oceanographic Abstracts* 13 (4): 607–620. ISSN: 0011-7471. doi:[https://doi.org/10.1016/0011-7471\(66\)90592-4](https://doi.org/10.1016/0011-7471(66)90592-4).
- Hunter, J. D. 2007. "Matplotlib: A 2D graphics environment". *Computing in Science & Engineering* 9 (3): 90–95. doi:10.1109/MCSE.2007.55.

- Jahnke, Annika, et al. 2017. "Reducing Uncertainty and Confronting Ignorance about the Possible Impacts of Weathering Plastic in the Marine Environment". *Environmental Science & Technology Letters* 4 (): doi:10.1021/acs.estlett.7b00008.
- Jambeck, Jenna R., et al. 2015. "Plastic waste inputs from land into the ocean". *Science* 347 (6223): 768–771. doi:10.1126/science.1260352.
- Jones, Eric, Travis Oliphant, Pearu Peterson, et al. 2001. *SciPy: Open source scientific tools for Python*. [Online; accessed 26.07.2019]. <http://www.scipy.org/>.
- Kaiser, David, Nicole Kowalski, and Joanna Waniek. 2017. "Effects of biofouling on the sinking behavior of microplastics". *Environmental Research Letters* 12 (): doi:10.1088/1748-9326/aa8e8b.
- Kooi, Merel, et al. 2016. "The effect of particle properties on the depth profile of buoyant plastics in the ocean". *Scientific Reports* 6 (): 1–10. doi:10.1038/srep33882.
- Kooi, Merel, et al. 2017. "Ups and downs in the ocean: Effects of biofouling on the vertical transport of microplastics". *Environmental Science & Technology* 51 (): doi:10.1021/acs.est.6b04702.
- Kukulka, T, et al. 2012. "The effect of wind mixing on the vertical distribution of buoyant plastic debris". *Geophysical Research Letters* 39 (): 7601–. doi:10.1029/2012GL051116.
- Lange, M., and E. Van Sebille. 2017. "Parcels v0.9: prototyping a Lagrangian ocean analysis framework for the petascale age". *Geoscientific Model Development* 10 (11): 4175–4186. doi:10.5194/gmd-10-4175-2017.
- Law, Kara Lavender, et al. 2010. "Plastic Accumulation in the North Atlantic Subtropical Gyre". *Science* 329 (5996): 1185–1188. doi:10.1126/science.1192321.
- Lebreton, Laurent, et al. 2018. "Evidence that the Great Pacific Garbage Patch is rapidly accumulating plastic". *Scientific Reports* 2018 (). doi:10.1038/s41598-018-22939-w.
- Lei, Lili, et al. 2017. "Microplastic particles cause intestinal damage and other adverse effects in zebrafish *Danio rerio* and nematode *Caenorhabditis elegans*". *The Science of the total environment* 619-620 (): 1–8. doi:10.1016/j.scitotenv.2017.11.103.
- Madec, G. 2008. *NEMO ocean engine*. Note du Pôle de modélisation, Institut Pierre-Simon Laplace (IPSL), France, No 27, ISSN No 1288-1619.
- Madec, Gurvan, and Maurice Imbard. 1996. "A global ocean mesh to overcome the North Pole singularity". *Climate Dynamics* 12 (): 381–388. doi:10.1007/BF00211684.
- M.C. Fazey, Francesca, and Peter Ryan. 2016. "Biofouling on buoyant marine plastics: An experimental study into the effect of size on surface longevity". *Environmental Pollution* 210 (): 354–360. doi:10.1016/j.envpol.2016.01.026.
- Nooteboom, Peter D., et al. 2019. "Transport bias by ocean currents in sedimentary microplankton assemblages: Implications for paleoceanographic reconstructions". *Paleoceanography and Paleoceanography* 0 (ja). doi:10.1029/2019PA003606.

- Onink, Victor, et al. 2019. “The Role of Ekman Currents, Geostrophy, and Stokes Drift in the Accumulation of Floating Microplastic”. *Journal of Geophysical Research: Oceans* 0 (0). doi:10.1029/2018JC014547.
- Poulain, Marie, et al. 2019. “Small Microplastics As a Main Contributor to Plastic Mass Balance in the North Atlantic Subtropical Gyre”. *Environmental Science & Technology* 53 (3): 1157–1164. doi:10.1021/acs.est.8b05458.
- Reisser, J., et al. 2015. “The vertical distribution of buoyant plastics at sea: an observational study in the North Atlantic Gyre”. *Biogeosciences* 12 (4): 1249–1256. doi:10.5194/bg-12-1249-2015.
- Ryan, Peter. 2015. “The importance of size and buoyancy for long-distance transport of marine debris”. *Environ. Res. Lett.* 10 () .
- Schudlich, Rebecca R., and James F. Price. 1998. “Observations of Seasonal Variation in the Ekman Layer”. *Journal of Physical Oceanography* 28 (6): 1187–1204. doi:10.1175/1520-0485(1998)028<1187:OOSVIT>2.0.CO;2.
- Sheng, Chen, et al. 2018. “Deviation of Wind Stress From Wind Direction Under Low Wind Conditions”. *Journal of Geophysical Research: Oceans* (). doi:10.1029/2018JC014137.
- Singh, Sohana P., et al. 2018. “Seascape genetics of the spiny lobster Panulirus homarus in the Western Indian Ocean: Understanding how oceanographic features shape the genetic structure of species with high larval dispersal potential”. *Ecology and Evolution* 8 (23): 12221–12237. doi:10.1002/ece3.4684.
- Van den Bremer, Ton, and Oyvind Breivik. 2018. “Stokes drift”. *Philosophical Transactions of The Royal Society A Mathematical Physical and Engineering Sciences* 376 (): 20170104. doi:10.1098/rsta.2017.0104.
- Van Sebille, Erik, et al. 2015. “A global inventory of small floating plastic debris”. *Environmental Research Letters* 10 (): 124006. doi:10.1088/1748-9326/10/12/124006.
- Weller, Robert A., and Albert J. Plueddemann. 1996. “Observations of the vertical structure of the oceanic boundary layer”. *Journal of Geophysical Research: Oceans* 101 (C4): 8789–8806. doi:10.1029/96JC00206.

8 Annexes

8.1 Figures

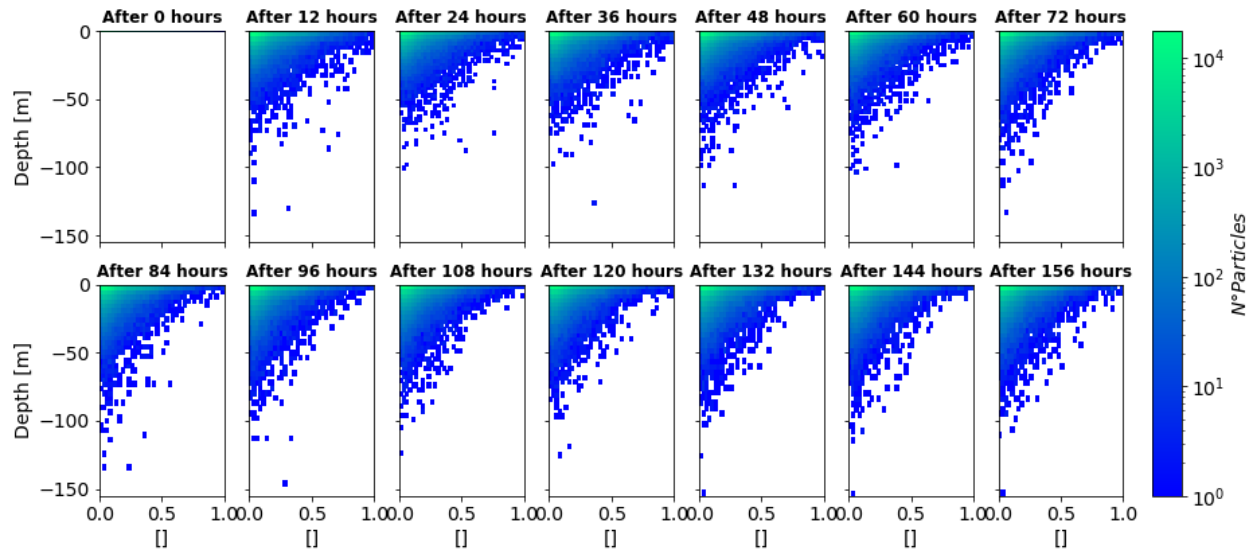


Figure 18: 2D Histogram of distance in normalised distanced [] versus Depth [m] - Kukulka simulation

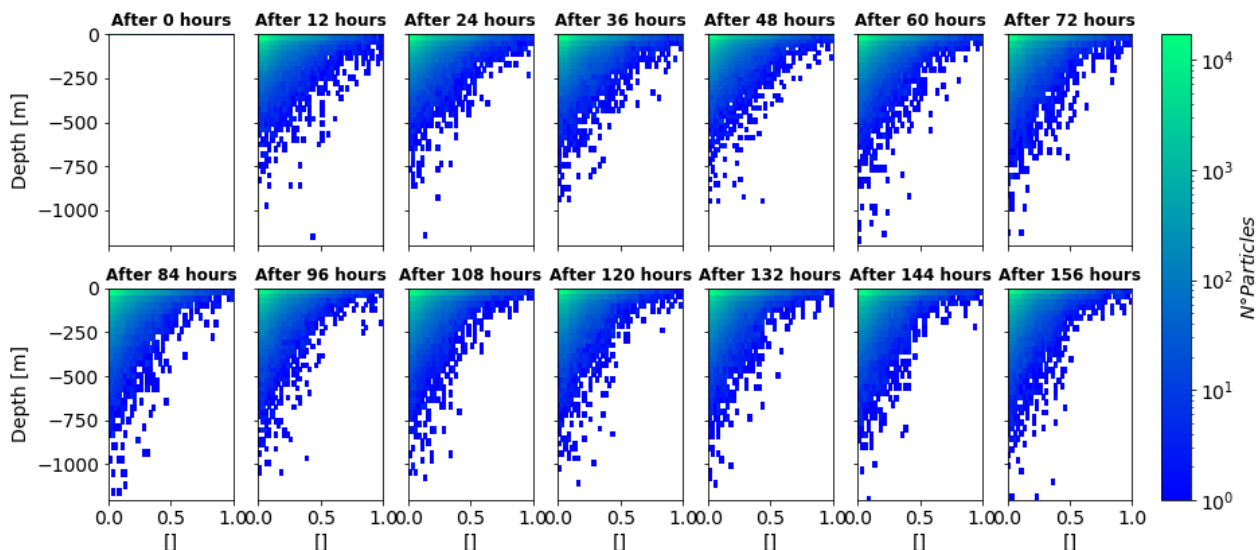
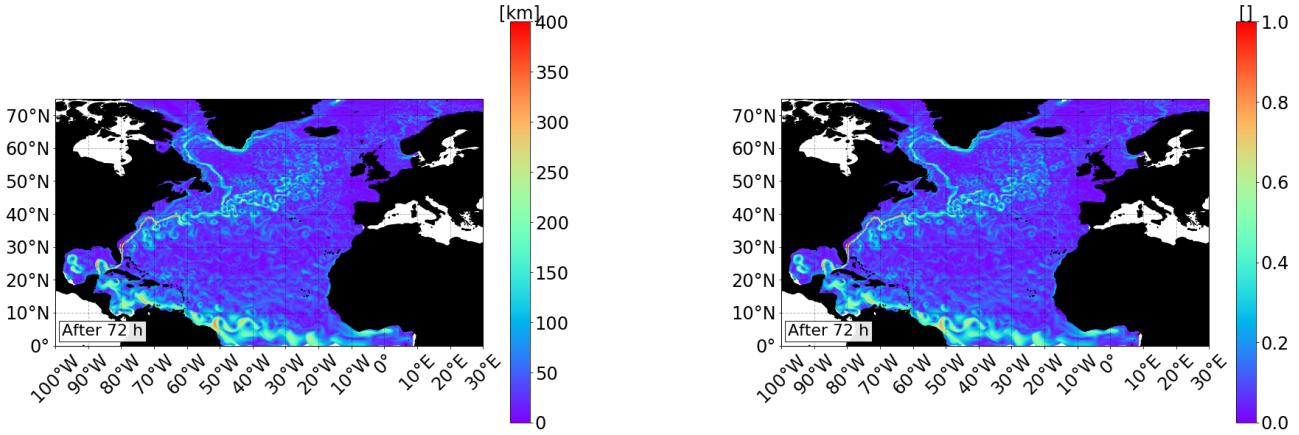
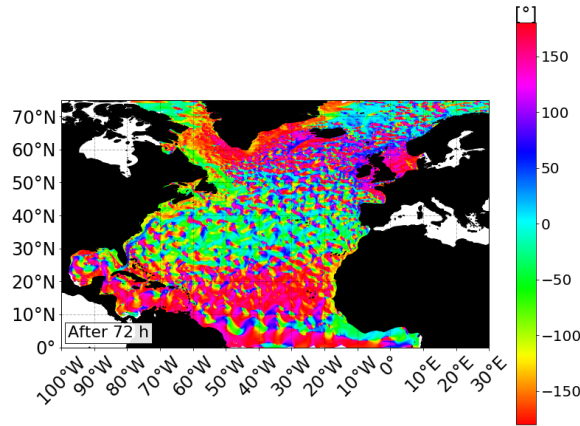


Figure 19: 2D Histogram of distance in normalised distanced [] versus Depth [m] - Poulain simulation



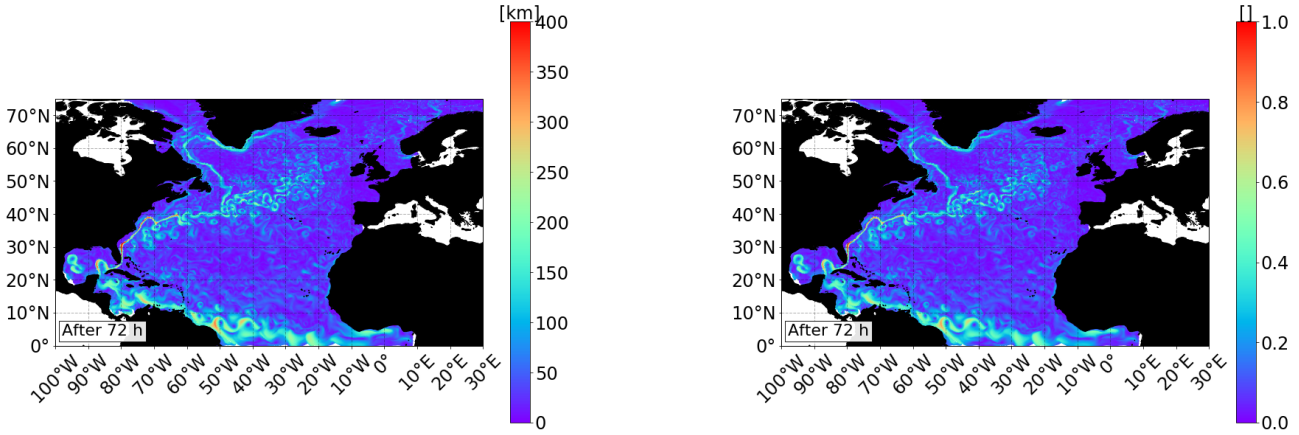
(a) Distances of advected particles from initial position after three days in [km].

(b) Distances of advected particles from initial position after three days in normalized units [].



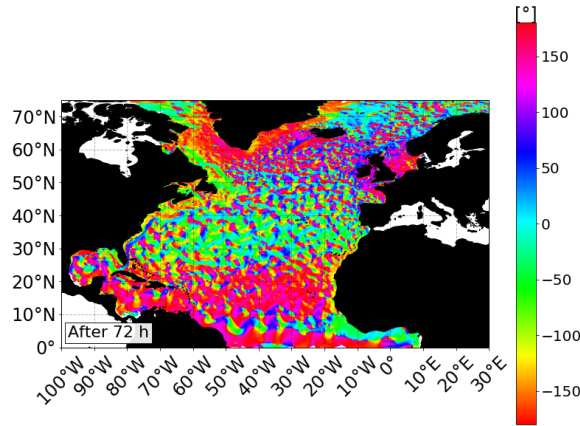
(c) Bearing of advected particles after three days in [°].

Figure 20: Polar coordinates (distances and bearing) of advected particles in surface simulation after three days. Note that 0° points eastwards.



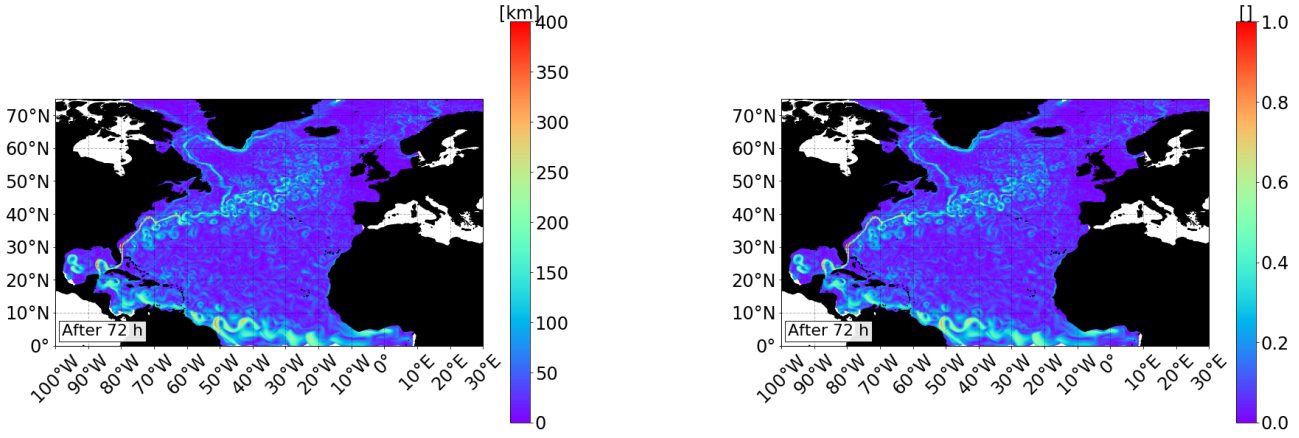
(a) Distances of advected particles from initial position after three days in [km].

(b) Distances of advected particles from initial position after three days in normalized units [].



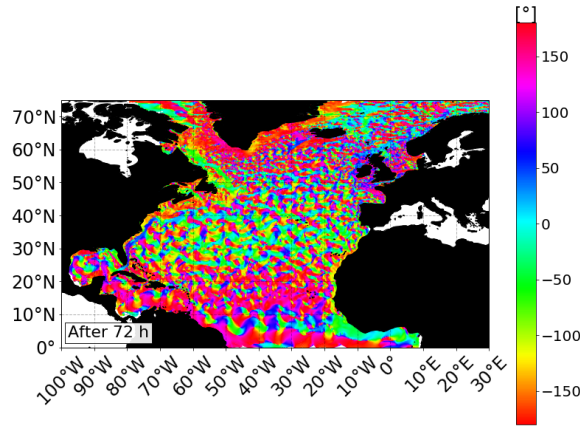
(c) Bearing of advected particles after three days in [°].

Figure 21: Polar coordinates (distances and bearing) of advected particles in Kukulka simulation after three days. Note that 0° points eastwards.



(a) Distances of advected particles from initial position after three days in [km].

(b) Distances of advected particles from initial position after three days in normalized units [].



(c) Bearing of advected particles after three days in [°].

Figure 22: Polar coordinates (distances and bearing) of advected particles in Poulain simulation after three days. Note that 0° points eastwards.

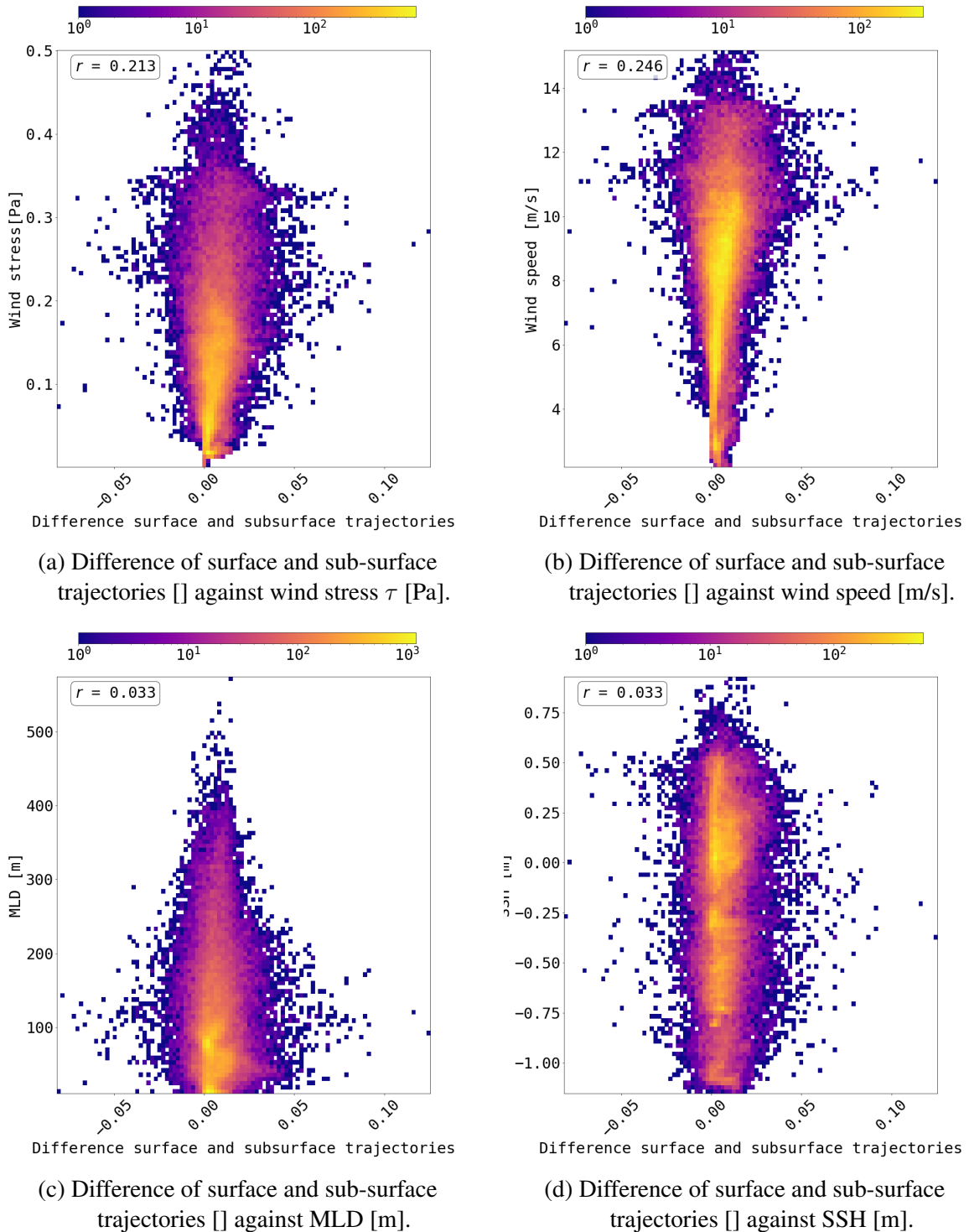


Figure 23: Kukulka mixing - North-Atlantic: Two-dimensional histograms of surface distances minus sub-surface distances [] against various NEMO variables. Additionally, the Pearson correlation r is calculated.

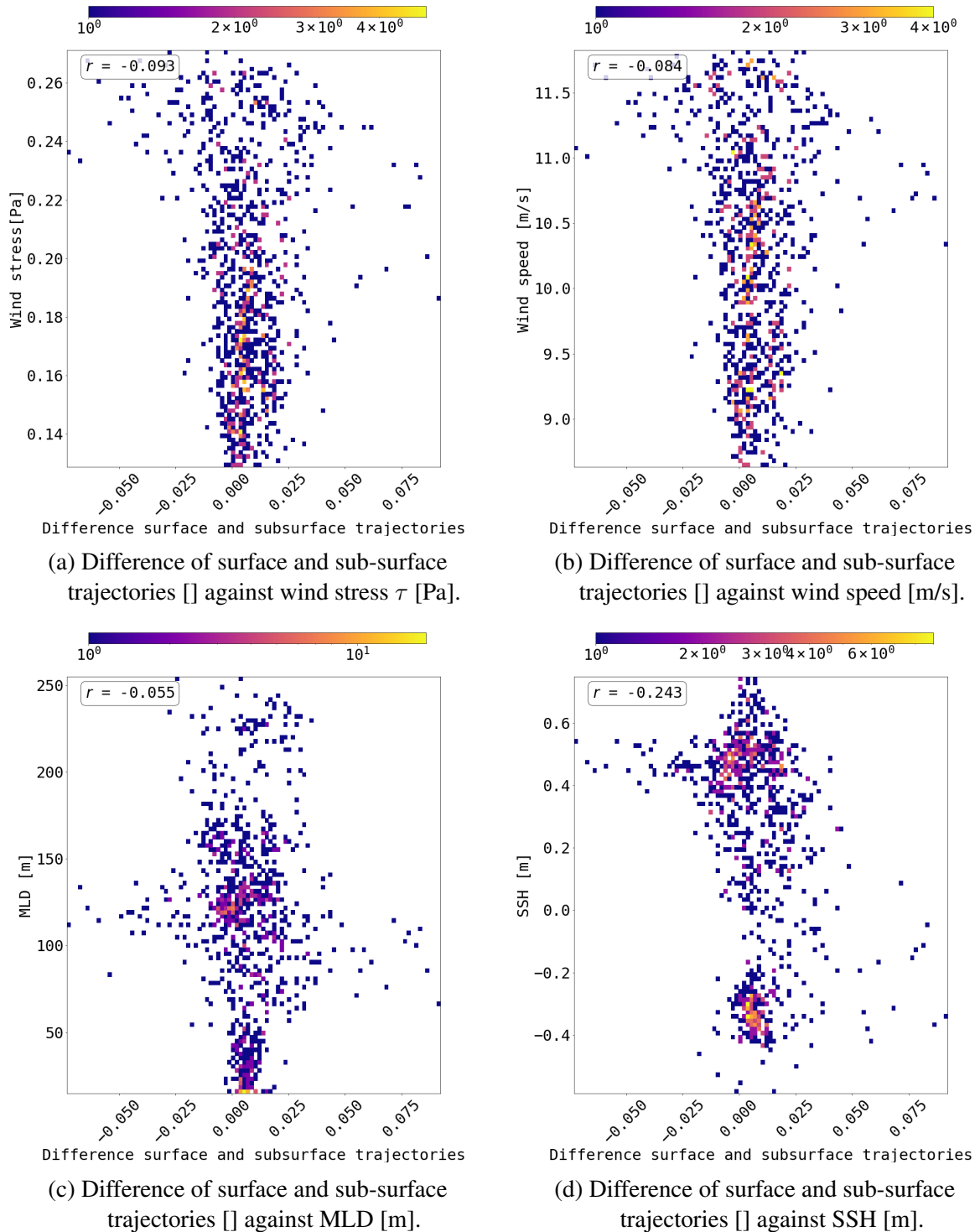


Figure 24: Kukulka mixing - Gulf stream: Two-dimensional histograms of surface distances minus sub-surface distances [m] against various NEMO variables. Additionally, the Pearson correlation r is calculated.

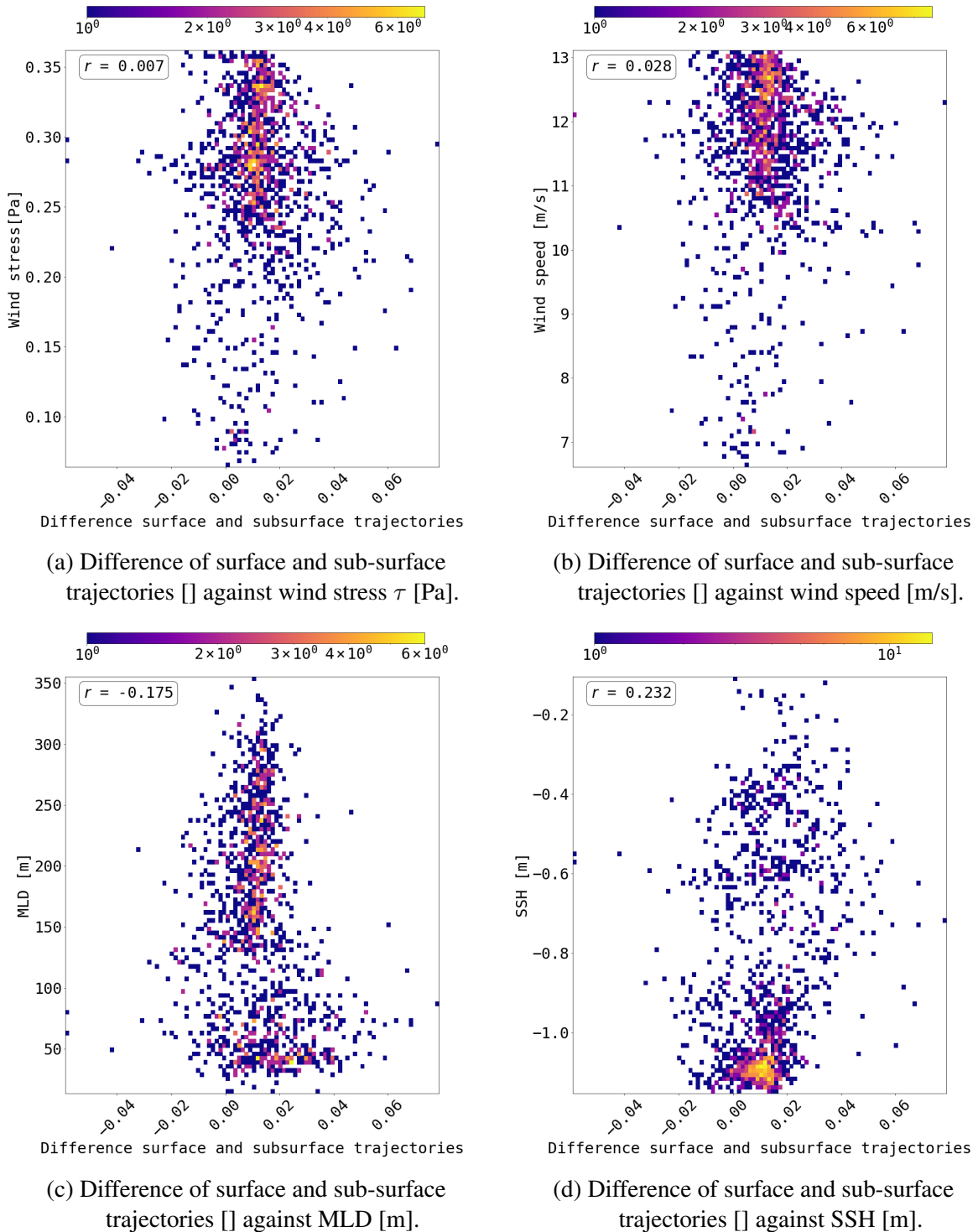


Figure 25: Kukulka mixing - Labrador sea: Two-dimensional histograms of surface distances minus sub-surface distances [] against various NEMO variables. Additionally, the Pearson correlation r is calculated.

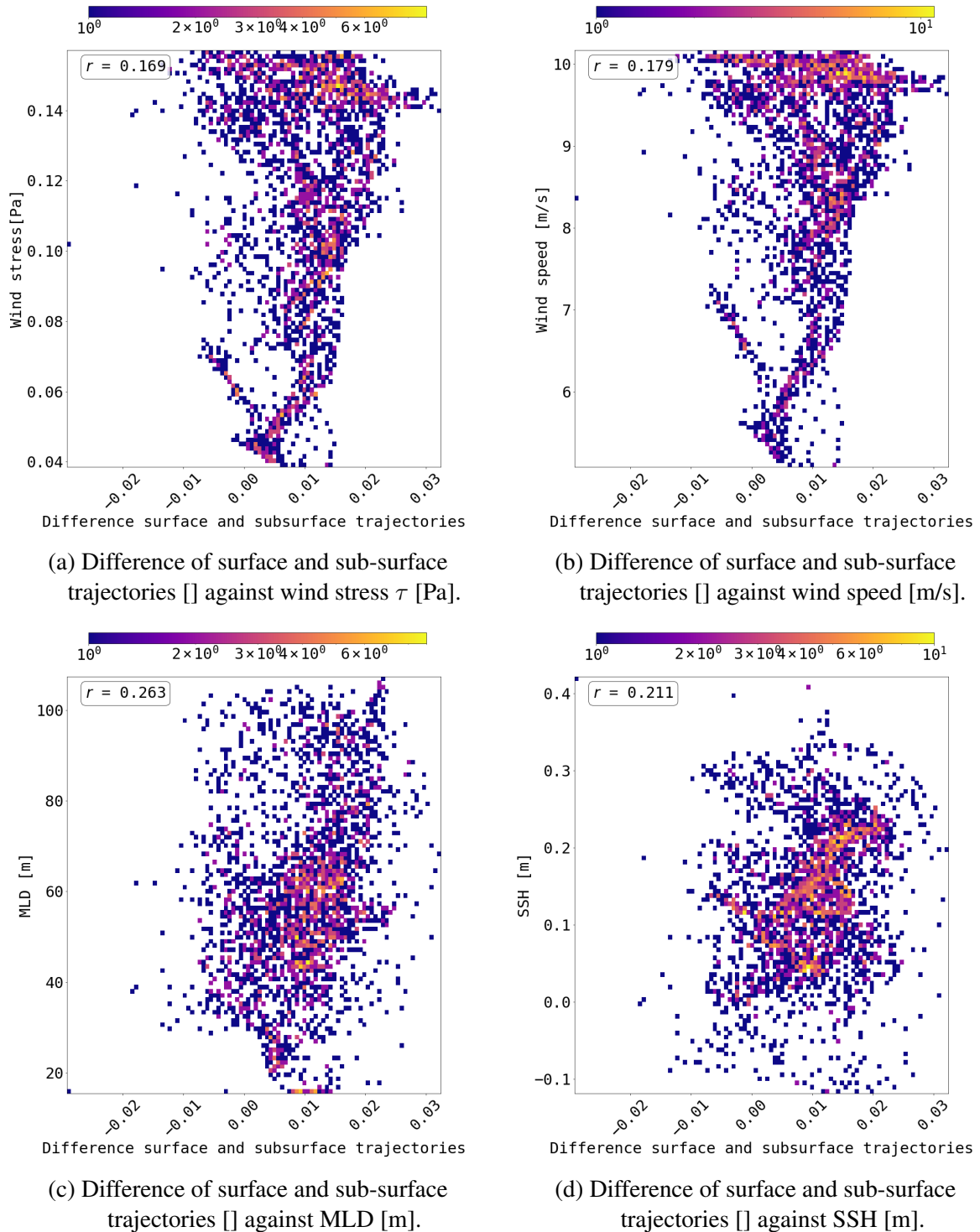


Figure 26: Kukulka mixing - Equatorial current: Two-dimensional histograms of surface distances minus sub-surface distances [] against various NEMO variables. Additionally, the Pearson correlation r is calculated.

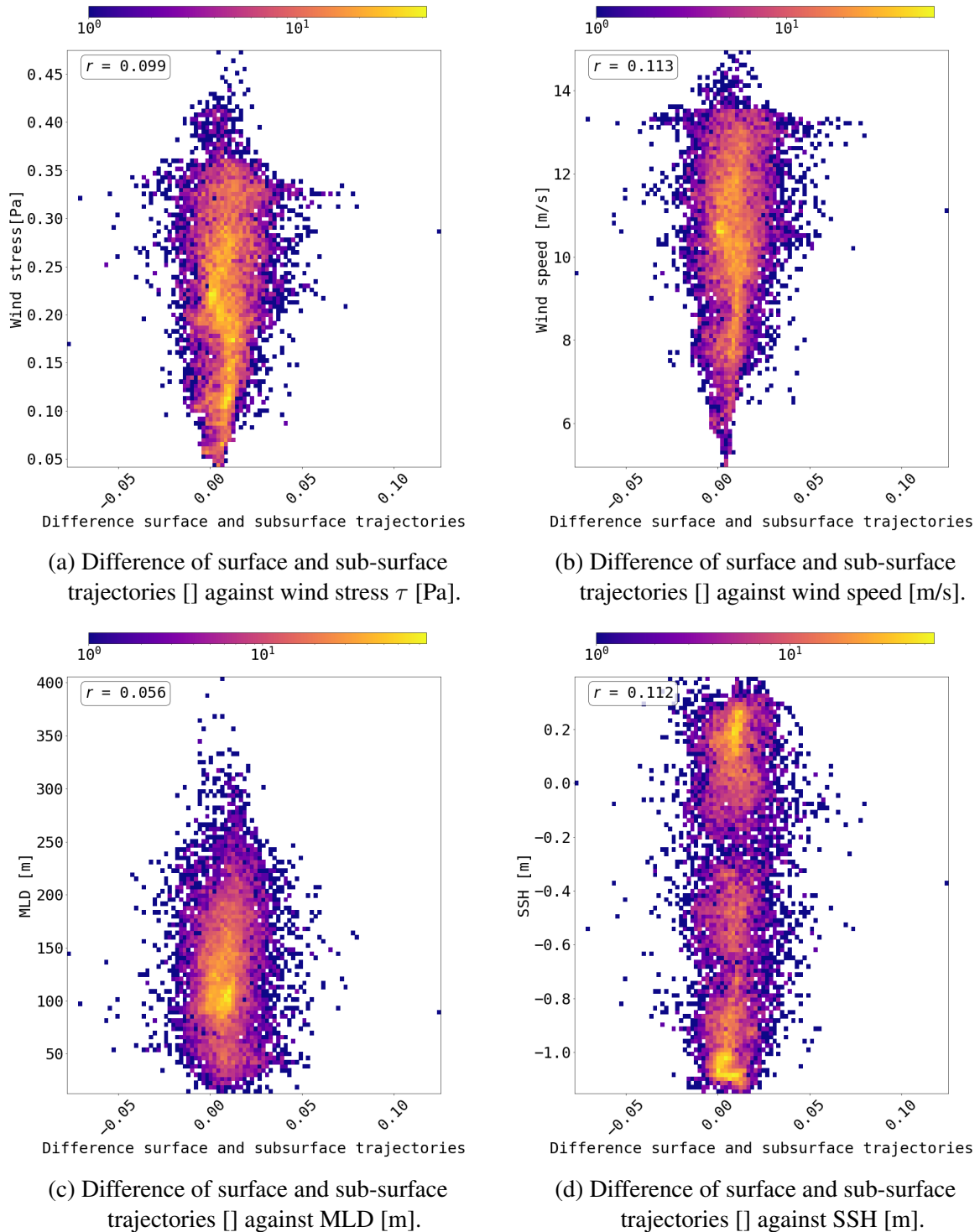


Figure 27: Kukulka mixing - Center: Two-dimensional histograms of surface distances minus sub-surface distances [] against various NEMO variables. Additionally, the Pearson correlation r is calculated.

8.2 Scripts

The scripts for the simulations, post-processing and plotting can be found in the github-repository: <https://github.com/judithmarinaewald/Master-thesis-project>

List of Figures

1	Spatial scales of SKIM measurements. From the smallest to the largest scale: The smallest scale represents the wind-generated wave data measured with Doppler technology. The circle represents a footprint with a diameter of 6 km. These footprints can be separated into azimuthal strips with a 300m-resolution which is indicated with the red boxes. One scale larger one can see the 320 km wide swath. The dots are the footprints which are sparsely distributed along the swath with a distance of 5 - 15 km to each other. Here, the black line shows the nadir radar beam, the coloured dots show the 12° incidence angle radar beams and the grey dots represent the 6° incidence angle radar beams as explained in the text. The image with the largest scale shows that the revisit time varies with latitudes. With a 824 km altitude orbit the revisit time is between 8 hours and 4 days. Source: Arduin et al. (2019)	7
2	Initial grid of the particles. a) Shows distribution of 122622 particles in North Atlantic; b) presents particles per bin: The distribution should be consistent everywhere but on land.	9
3	Travelled distances (a, b) and change in angles (c, d) of 270 particles after 3 days. Particles are released simultaneously from two lines: (1) 35° N and 65° - 75° W; (2) 3° N and 65° - 80° W.	13
4	Differences in distances (a, b) and angles (c) after 3 days. The markers represent the particle positions of the surface simulation after three days, and the colorbar shows the difference of surface and sub-surface simulation. In (a, b) positive values indicate larger travelled distances of surface particles than sub-surface particles and vice versa. In (c) a change of direction is represented by the absolute difference between the angles of surface and sub-surface simulations (figure 3 c, d).	14
5	Histogram of particle distribution over depth for simulation 'Poulain'	16
6	Histogram of particle distribution over depth for simulation 'Kukulka'	16
7	Particle Depths (m) after a simulation run of 3 days. Note the different depth scales of the Kukulka (a) and Poulain (b) simulation.	17
8	Differences of surface and sub-surface distances after 3 days for the North Atlantic. Positive distances indicate that surface distances are larger than sub-surface distances and vice versa. Note the different scales of (a, b).	18
9	2D Histogram of distance in [km] versus depth [m] - Kukulka simulation . . .	19
10	2D Histogram of distance in [km] versus depth [m] - Poulain simulation . . .	19
11	Differences of surface and sub-surface directions after 3 days for the North Atlantic. Note that the differences are in absolute values, hence they only indicate the absolute change of direction, but not the orientation.	20

12	Various NEMO variables: 5-day means simultaneous with PARCELS simulations (compare table 1)	22
13	Poulain mixing - North-Atlantic: Two-dimensional histograms of surface distances minus sub-surface distances [] against various NEMO variables. Additionally, the Pearson correlation r is calculated.	23
14	Poulain mixing - Gulf stream: Two-dimensional histograms of surface distances minus sub-surface distances [] against various NEMO variables. Additionally, the Pearson correlation r is calculated.	24
15	Poulain mixing - Labrador sea: Two-dimensional histograms of surface distances minus sub-surface distances [] against various NEMO variables. Additionally, the Pearson correlation r is calculated.	25
16	Poulain mixing - Equatorial current: Two-dimensional histograms of surface distances minus sub-surface distances [] against various NEMO variables. Additionally, the Pearson correlation r is calculated.	26
17	Poulain mixing - Center: Two-dimensional histograms of surface distances minus sub-surface distances [] against various NEMO variables. Additionally, the Pearson correlation r is calculated.	27
18	2D Histogram of distance in normalised distanced [] versus Depth [m] - Kukulka simulation	37
19	2D Histogram of distance in normalised distanced [] versus Depth [m] - Poulain simulation	37
20	Polar coordinates (distances and bearing) of advected particles in surface simulation after three days. Note that 0° points eastwards.	38
21	Polar coordinates (distances and bearing) of advected particles in Kukulka simulation after three days. Note that 0° points eastwards.	39
22	Polar coordinates (distances and bearing) of advected particles in Poulain simulation after three days. Note that 0° points eastwards.	40
23	Kukulka mixing - North-Atlantic: Two-dimensional histograms of surface distances minus sub-surface distances [] against various NEMO variables. Additionally, the Pearson correlation r is calculated.	41
24	Kukulka mixing - Gulf stream: Two-dimensional histograms of surface distances minus sub-surface distances [] against various NEMO variables. Additionally, the Pearson correlation r is calculated.	42
25	Kukulka mixing - Labrador sea: Two-dimensional histograms of surface distances minus sub-surface distances [] against various NEMO variables. Additionally, the Pearson correlation r is calculated.	43
26	Kukulka mixing - Equatorial current: Two-dimensional histograms of surface distances minus sub-surface distances [] against various NEMO variables. Additionally, the Pearson correlation r is calculated.	44

27	Kukulka mixing - Center: Two-dimensional histograms of surface distances minus sub-surface distances [] against various NEMO variables. Additionally, the Pearson correlation r is calculated.	45
----	--	----